Effect of the heave plate's diameter on the transitional motions of a straked marine circular cylinder (MCC) under different marine conditions

Mahdi Bandizadeh Sharif[a,b], Hassan Ghassemi[b,c*], Guanghua He (何广华)[c], Pengfei Liu (刘鹏飞)[d]

[a]Department of Civil and Environmental Engineering, Amirkabir University of Technology, Tehran, Iran.
[b]Department of Maritime Engineering, Amirkabir University of Technology, Tehran, Iran.
[c]Int. School of Ocean Science and Engineering, Harbin Institute of Technology, Weihai, China.
[d]School of Engineering, Newcastle University, Newcastle upon Tyne, UK.
[*]Corresponding author. E-mail address: gasemi@aut.ac.ir (H. Ghassemi)

Abstract

This numerical study investigated the influence of the heave plate's diameter on the amplitude of the transitional motions of a Marine Circular Cylinder (MCC) with a low aspect ratio under the marine current and regular waves. Due to the experimental model of the straked MCC, different diameters of the circular heave plate were chosen to be installed at the keel of the 3-straked MCC. In this numerical study, the diameter of the heave plate varied from $1.2D_{MCC}$ to $1.6D_{MCC}$, while other parameters, such as reduced velocity (V_R), Reynolds (Re) number, and Froude number, were kept constant. In this study, the transitional motions, including surge, sway, and heave, were analysed. The results showed that increasing the heave plate's diameter decreased the amplitude of the transitional motions in both marine current and regular waves. Also, the finding revealed that the heave plate not only reduced the amplitude of the heave motion but also decreased the amplitude of surge and sway motions. Moreover, the outcomes indicated that the heave plate's diameter increased by approximately 20-40% more than the MCC's diameter. This caused the smaller amplitude of the transitional motions under both marine currents and regular waves.

Keywords: Marine circular cylinder (MCC), Circular heave plate, Transitional motions, Marine current, Regular waves, Numerical modeling.

1. Introduction

This study uses numerical simulation to explore the potential advantages and efficiency of using both a heave plate and a strake plate to suppress the transitional motions of a Marine Circular Cylinder (MCC). Hence, to provide a comprehensive analysis, the literature review of each component, heave plate and strake plate, will be separately discussed and examined. Hence, a clearer understanding of their characteristics and potential synergies can be gained, ultimately contributing to advancing knowledge in this area.

1.1. Heave plate

Recent studies have indicated that using the heave plates in offshore structures effectively minimizes the transitional motions and the Vortex-Induced Motion (VIM) response of the

MCCs by Gonçalves et al., (2020, 2022, and 2023), due to the non-dimensional parameters, such as the Keulegan-Carpenter (KC) number, frequency (β), and reduced velocity (V_R) (Halkyard et al., 2002; Ishihara et al. 2009; Lam et al. 2010; Li et al. 2013; Liang et al. 2018; Jang et al. 2019). Lake et al., (2000) conducted experimental research to examine the effects of using attached and unattached heave plates at the keel of the MCC on the heave motion. The results showed that attaching heave plates at the keel of the MCC increased the hydrodynamic coefficients of the structure. Then Thiagarajan et al., (2002) conducted a study using both numerical simulations and experimental research to investigate the effects of heave plates with different diameters on reducing heave motion. The study found that using heave plates improved the hydrodynamic coefficients compared to the bare MCC. Additionally, increasing the heave plate's diameter decreased the heave motion by increasing the hydrodynamic coefficients. Also, Tao and Cai, (2004) performed a numerical study on an MCC with a heave plate. They found that the added mass at the keel was equivalent to a sphere with the diameter of the heave plate. Moreover, Sudhakar and Nallayarasu (2011) conducted an experiment to study the impact of marine currents on the MCC. They compared the motion of the platform with and without a heave plate using the ANSYS-AQWA. The results showed that the heave plate increased the heave damping and added mass coefficients of the structure by trapping a significant amount of water at the keel of the MCC. The study suggested that an optimal response was achieved when the heave plate's diameter was 20-40% larger than the MCC's diameter (D_{HP}=1.2-1.4D_{MCC}).

Sudhakar and Nallayarasu, (2013 and 2014) tested models of the MCC with different configurations, including a bare MCC and an MCC with different diameters of heave plate at the keel under regular waves. The results showed that increasing the heave plate's diameter by 20-30% compared to the MCC's diameter resulted in the greatest reduction in the heave response of the MCC. Then Li et al., (2013) investigated the effects of a heave plate on the heave motion of an MCC. They conducted model tests and numerical simulations, which confirmed that the heave plate effectively decreased the amplitude of the heave motion and improved the platform's stability. Tian et al., (2013) conducted a study on a heave plate that was oscillating in water to examine the impact of various parameters on its hydrodynamic performance. The results showed that the heave plate could generate significant hydrodynamic forces. The shape of the heave plate influenced hydrodynamic coefficients, with round, octagon, and hexagon plates having similar added mass coefficients, while the square plate had a lower added mass coefficient. Nallayarasu and Bairathi, (2014) conducted a study to evaluate the heave response of the MCC with a circular heave plate. The outcomes revealed that the presence of the heave plate had a positive effect on the hydrodynamic coefficients and significantly reduced the heave motions of the MCC. In addition, Lopez-Pavon et al., (2014) and Lopez-Pavon and Souto-Iglesias (2015) conducted experimental and numerical research to examine the impact of different circular heave plate configurations on the hydrodynamic coefficients under constant environmental conditions. The results showed that the simple heave plate exhibited higher values of added mass and damping compared to the reinforced heave plate.

Subbulakshmi et al., (2015) explored the numerical simulation about the impact of the heave plate's diameter on the heave Response Amplitude Operation (RAO) response of an MCC. The

finding indicated that the incorporation of the heave plate at the keel of the MCC decreased the heave RAO response by 33% and 37% at the D_{HP}/D_{MCC} of 1.2-1.3 and 1.4-1.5, respectively. Then Subbulakshmi and Sundaravadivelu, (2016 and 2021) carried out experimental and numerical research to investigate the effect of the diameter ratio (heave plate diameter to MCC diameter, D_{HP}/D_{MCC}) and position of the heave plates. The findings revealed that increasing the diameter ratio from 1 to 2 leads to an increase in added mass, resulting in a decrease in the heave RAO response and the most effective position for a single heave plate is at the keel of the MCC (Yue et al., 2020; Rao et al., 2021; Ali et al., 2021). In addition, Moreno et al., (2016) conducted numerical and experimental research to determine the hydrodynamic coefficients of different shapes of heave plates. Circular, hexagonal, and square shapes were chosen for the study and attached to the keel of an MCC. The results showed that the hydrodynamic coefficients were influenced by the heave plate geometry. Both the hexagonal and circular heave plates experienced higher hydrodynamic coefficients compared to the square heave plate.

Zhu and Lim, (2017) conducted experimental research to evaluate the effect of the heave plate's diameter on the hydrodynamic coefficients of an MCC. The results demonstrated that increasing the diameter of the heave plate was found to be more effective in reducing the heave RAO response of the MCC. The heave RAO response of the MCC with an optimal diameter (D_{HP}/D_{MCC} = 1.2-1.4) was 40% less than the bare MCC. Then Gonçalves et al., (2020, 2022, and 2023) investigated the impact of different heave plate designs on reducing the transitional motions and VIM response of an MCC with a low aspect ratio. The study focused on the effects of the heave plate's diameter on the hydrodynamic coefficients of the MCCs. The results showed that increasing the heave plate's diameter increased the hydrodynamic coefficients. The most effective heave plate's diameter for reducing In-Line (IL) and Cross-Flow (CF) displacement was found to have diameter ratios of (D_{HP}/D_{MCC} = 1.20-1.60). Additionally, Mello et al., (2019 and 2021)'s research indicated that changes in the diameter of heave plates had the greatest impact on added mass and damping coefficients, which caused a reduction in the heave RAO response of the MCC. Zhang and Ishihara, (2018 and 2020) carried out a numerical simulation to study the hydrodynamic forces acting on a circular heave plate. They used the Large-Eddy Simulation (LES) and Volume of Fluid (VOF) methods to model the Fluid-Structure Interaction (FSI). The results showed that the MCC with a heave plate had less heave motion compared to the bare MCC.

Ciba, (2021) and Ciba at el., (2022) performed numerical and experimental research to evaluate the hydrodynamic coefficients of an MCC with a heave plate. They utilized the Free Decay Test (FDT) and Computational Fluid Dynamic (CFD) methods with STAR-CCM+ software in both experimental and numerical research. The results showed that the MCC with the heave plate experienced lower heave motion due to induced damping and added mass coefficients in the governing equation. Furthermore, Ali et al., (2021) showed that the heave damping of the MCC increased by up to 49% when the heave plate, which had a size of 1.3-1.4D_{MCC}, was added to the keel of the MCC. Finally, Hegde and Nallayarasu, (2022 and 2023) performed experimental and numerical research to calculate the hydrodynamic characteristics of an MCC using different heave plate configurations. It was found that the optimal location for the heave plate was at the MCC's keel. Increasing the diameter ratio (D_{HP}/D_{MCC}) resulted in higher added

mass and heave damping coefficients and led to a decrease in the heave RAO response of the MCC.

1.2. Strake plate

Finn et al., (2003) conducted studies on an MCC to reduce the VIM response by using strake plates. The research showed that using the str ake plates on the MCC's hull significantly reduced the VIM phenomenon in the structure. The optimal strake plate had a height of 10% to 14% of the MCC's diameter by Irani and Finn (2004). Then DeMerchant et al., (2005) utilized numerical modeling to investigate MCC's VIM response and fatigue under the strong marine currents in the Gulf of Mexico (GoM). The findings showed that increasing the height of the strake plates to an optimal value reduced both VIM and fatigue. The research conducted by Halkyard et al., (2005 and 2006) demonstrated that the CFD method can be used to predict the VIM and transitional motions in the MCCs. The simulation was done at a model scale of 1:40, with a Re number ranging from 4×10^4 to 15×10^4 and a V_R range of 3 to 11. The results showed that the VIM response was reduced by about 88% for the straked MCC compared to the bare MCC. Furthermore, Thiagarajan et al., (2005) conducted a study using the CFD method to investigate the impact of strake plates on reducing VIM response. The height of the strake plates was determined to be 13% of the MCC's diameter, and the strake plates were symmetrically arranged at an angle of 120 degrees around the MCC's hull. The results demonstrated that straked MCC resulted in a reduction in VIM response. The importance of incorporating additional details, such as chains, anodes, and tubes, and utilizing a fine mesh in the CFD method to ensure accuracy was discussed by Atluri et al., (2006).

Tallavajhula et al., (2007) evaluated the effect of the strake plates on the VIM and fatigue damage of an MCC. The results revealed that the height, quantity, and pitch of the strake plates were crucial in mitigating VIM response and fatigue damage. Also, Irani and Perryman (2008 and 2005) investigated the impact of VIM on an MCC, comparing the numerical and experimental results of a straked MCC and a bare MCC. The findings showed that strake plates reduced the VIM response of the MCC by preventing the formation of the vortex shedding behind the straked MCC. Wang et al., (2010) employed the CFD method to model the flow around the straked MCC. The height of the strake plates was set at 14% of the MCC's diameter. Comparing the results of the bare cell MCC and the cell MCC with strake plates, it was observed that the strake plates altered the pressure distribution on the MCC's hull. In the bare structure, the maximum pressure occurred at the back of the hull due to reverse flow, while in the straked MCC, the pressure in that area was significantly reduced, with the maximum pressure occurring on the strake plates. The study demonstrated that the use of strake plates effectively suppressed the VIM response by eliminating vortex shedding in the wake layer of the straked MCC. Then Ding and Li (2017) and Ding et al., (2017) performed numerical research on an MCC platform to study the effect of helical strake plates on the transitional motions of the MCC. The results showed that the reduction of the MCC's RAO response was greatly depended on the strake's height and pitch.

Holland et al., (2017) used the Star CCM+ software and combined the Detached Eddy Simulation (DES) model with the Reynolds-Averaged Navier-Stokes (RANS) model to

evaluate vortex shedding patterns around the straked MCC. The findings showed that in the absence of strake plates, vortex shedding increased symmetrically, leading to structural vibrations. However, when strake plates were used on the MCC, vortex shedding decreased and occurred at the edges of the strakes, resulting in a less symmetrical shedding pattern and a reduced VIM response of the MCC. Furthermore, Carlson and Sadeghi (2018) conducted experimental research to investigate the VIM of an MCC. They used four different models of the MCC's hull, including a bare MCC, a fully straked MCC, an upper-straked MCC, and a lower-straked MCC. The findings showed that the MCC was covered by lower and fully straked MCC, the VIM response was significantly reduced, and the lock-in phenomenon did not occur. Fernandes et al., (2021) conducted a study to investigate the impact of a helical strake on Von Kármán vortex street in the marine environment. Findings demonstrated that the presence of strakes helped suppress the formation of vertex shedding in downstream by widening the wake layer and preventing interference between shear layers on the sides of the structure. Finally, Kharazmi and Ketabdari (2022) used a model developed by Finnigan and Roddier (2007) to numerically analyze and determine the optimal number and angles of strake plates on an MCC with a low aspect ratio. The findings revealed that a pattern consisting of three strake plates at 120 degrees has the best performance in reducing the amplitude of the transitional motions.

2. Governing equation

2.1. Free decay test (FDT)

The equation for the free decay test (FDT) of an MCC under three transitional motions is as follows (Ciba et al., 2021; Ciba et al., 2022; Ciba et al., 2023):

$$(M + M_a)\ddot{A} + C\dot{A} + KA = 0 \tag{1}$$

$$\ddot{A} + 2\eta\dot{A} + {\omega_n}^2 A = 0 \tag{2}$$

$$\begin{Bmatrix} A \\ \dot{A} \\ \ddot{A} \end{Bmatrix} = \begin{Bmatrix} X & Y & Z \\ \dot{X} & \dot{Y} & \dot{Z} \\ \ddot{X} & \ddot{Y} & \ddot{Z} \end{Bmatrix} \tag{3}$$

$$\eta = \frac{C}{C_0} = \frac{C}{2\sqrt{K(M + M_a)}} \tag{4}$$

$$\bar{A} = \left(\frac{A_{(i)} - A_{(i+1)}}{A_{(i+2)} - A_{(i+3)}} \right) \tag{5}$$

$$\eta = \frac{1}{2\pi} \times ln(\bar{A}) \tag{6}$$

$$K = \rho_w g S_{WP} \tag{7}$$

$$S_{wp} = \frac{\pi D^2}{4} \tag{8}$$

$$M = \Delta = \rho_w \nabla = \frac{1}{4}\rho_w g \pi D^2 T \tag{9}$$

$$\omega_n = \sqrt{\frac{K}{M + M_a}} \tag{10}$$

$$\omega_d = \omega_n \sqrt{1 - \eta^2} \tag{11}$$

$$T_d = \frac{T_n}{\sqrt{1-\eta^2}} \tag{12}$$

$$A(t) = e^{-\eta\omega_n t}(A_0 cos\omega_d t + \frac{\dot{A}_0 + \eta\omega_n A_0}{\omega_d} sin\omega_d t) \tag{13}$$

where, {X Y Z} represent the surge, sway, and heave motions of the MCC, the velocity vector $\{\dot{X}\ \dot{Y}\ \dot{Z}\}$ is the derivative of the position vector with respect to time in the X, Y, and Z respectively, and the acceleration vector $\{\ddot{X}\ \ddot{Y}\ \ddot{Z}\}$ is the second derivative of the position vector with respect to time in the X, Y, and Z respectively.

2.2. Transitional motions

The equation that describes the motion of an MCC under the marine current and regular waves is as follows (Agarwal and Jain, 2003 and Soeb et al., 2017):

$$[M]\begin{Bmatrix}\ddot{X}\\ \ddot{Y}\\ \ddot{Z}\end{Bmatrix} + [C]\begin{Bmatrix}\dot{X}\\ \dot{Y}\\ \dot{Z}\end{Bmatrix} + [K]\begin{Bmatrix}X\\ Y\\ Z\end{Bmatrix} = \begin{Bmatrix}F_X(t)\\ F_Y(t)\\ F_Z(t)\end{Bmatrix} \tag{14}$$

$$[M] = [M]^{Structural\ mass} + [M]^{Added\ mass} \tag{15}$$

$$[C] = [C]^{Structural\ damping} + [C]^{Hydrodynamic\ damping} \tag{16}$$

$$[K] = [K]^{Elastic} + [K]^{Geometric} \tag{17}$$

here, {X Y Z} represent the surge, sway, and heave motions of the MCC, {F_X (t), F_Y (t), F_Z (t)} are the total force on the MCC + Spring damper system in the surge, sway, and heave motions respectively, while the velocity vector $\{\dot{X}\ \dot{Y}\ \dot{Z}\}$ is the derivative of the position vector with respect to time, and the acceleration vector $\{\ddot{X}\ \ddot{Y}\ \ddot{Z}\}$ is the second derivative of the position vector with respect to time. The total mass [M] is concentrated at the center of gravity of the MCC's mass and added mass. Also, the stiffness matrix [K] comprises of the elastic stiffness matrix and the geometric stiffness matrix. Moreover, the damping [C] consists of both structural and hydrodynamic damping, with the hydrodynamic effects being the main source of damping (Agarwal and Jain, 2003 and Soeb et al., 2017).

$$\varphi^T[C]^{Structural} = [2\xi\omega_i m_i] \tag{18}$$

$$[M_s + M(\infty)]\ddot{X}(t) + [C]\dot{X}(t) + [K]X(t) = F_{Morison} + F_{HSn} + F_M + F_e \tag{19}$$

In this scenario, F_H represents non-linear restoring forces, $F_{Morison}$ represents hydrodynamic forces caused by the inertia, drag force from waves, and current loading, M (∞) represents the added mass matrix, and Fe includes non-linear forces from the translational motion equations of the 3 DOF rigid MCC hull, with M_S being its 3×3 mass matrix. The force on the mooring line (spring damper), F_M, is accounted for in a consistent manner. The Morison's equation is considered sufficient for calculating hydrodynamic forces. The wave loads on the structure are determined by integrating forces along the free surface centerline from the bottom to the current position of the free surface (Agarwal and Jain, 2003 and Soeb et al., 2017). Wave theories are used to determine various aspects of waves in the sea, such as the motion and speed of water particles, the height and period of the waves, and the depth of the water. For this study, the

regular wave theory has been used to express the kinematics of particles as φ (Agarwal and Jain, 2003 and Soeb et al., 2017).

$$\varphi = \frac{\pi H}{kT}\frac{\cos k(z+d)}{\cosh(kd)}\sin(kx-\omega t) \quad (20)$$

$$u = \frac{\partial \varphi}{\partial x} = \frac{\pi H}{T}\frac{\cos k(z+d)}{\sin h(kd)}\cos(kx-\omega t) \quad (21)$$

$$w = \frac{\partial \varphi}{\partial z} = \frac{\pi H}{T}\frac{\sin k(z+d)}{\sin h(kd)}\sin(kx-\omega t) \quad (22)$$

$$\dot{u} = \frac{\partial u}{\partial t} = \frac{2\pi^2 H}{T^2}\frac{\cos k(z+d)}{\sin h(kd)}\sin(kx-\omega t) \quad (23)$$

$$\dot{w} = \frac{\partial w}{\partial t} = \frac{2\pi^2 H}{T^2}\frac{\sin k(z+d)}{\sin h(kd)}\cos(kx-\omega t) \quad (24)$$

which, *H, k, T, ω,* and *d* correspond to the wave height, wave number, wave period, angular frequency, and water depth, respectively. Also, u and w are the horizontal and vertical velocities, $\dot{u}$ and $\dot{w}$ represent accelerations of the flow in the horizontal and vertical directions.

3. Numerical implementation

3.1. Experimental models

Three different model scales have been constructed for the prototype of the straked MCC with a low aspect ratio as the Gulf of Mexico (GoM) spars. These models were built at the University of California (UC) at Berkeley, Force Technology (FT), and David Taylor Model Basin (DTMB) at the scales of 1:142.8, 1:65, and 1:22.3, respectively. The model built at the DTMB was chosen for this numerical study due to its large scale. Hence, Oakley et al., (2005 and 2007) examined the effects of various components, such as strake plates, pipes, chains, and anodes, on a scaled model of a bare MCC. The study used a numerical modeling technique called DES to reduce computational costs. The results indicated that the presence of strake plates and other attachments influenced the VIM response and vortex patterns around the straked MCC. Additionally, Finnigan and Roddier (2007) demonstrated that more detailed models, whether in the laboratory or through numerical modeling, yielded more accurate results in measuring the amplitude of the transitional motions. The study aimed to compare the amplitude of the transitional motions of the MCC equipped with various components and strake plates at supercritical Re numbers. The results demonstrated that including components such as pipes, chains, and anodes in the model effectively mitigated the amplitude of the transitional motions of the MCC. Then Roddier et al. (2009) conducted experimental research to examine the impact of the Re number and the various components of an MCC's hull on the VIM phenomenon. They tested three MCC models at different angles and reduced velocities (V_R) to evaluate the effect of hull components and flow angles on the amplitude of the MCC's motions. The findings showed that the performance of strake plates in reducing the VIM response depended on the flow angle. Also, the MCC's components played a noticeable role in suppressing the VIM response. Furthermore, Lefevre et al. (2012) conducted a numerical study on an MCC with strake plates, pipes, chains, and anodes to assess the amplitude of the surge and sway motions of the MCC. The study was modeled using CFD based on previous research

by Finnigan and Roddier (2007) and Roddier et al. (2009). The MCC's hull and its components were meshed using both fine and coarse meshing. The results of the CFD simulation indicated that the finer meshing provided a more accurate response compared to the coarser meshing. Nevertheless, Fig. 1 shows different configurations regarding the placement of various components on the MCC's hull. In the base case, all appurtenances such as chains, pipes, anodes, and strakes are present on the hull, as displayed in Fig. 1(a). Due to Fig. 1(b) in Variation-1, the chains and pipes are removed, but the model still includes strakes, anodes, and fairleads. Based on Fig. 1(c) in Variation-2, the bare MCC is only equipped with the three strakes with an angle of 120 degrees around the MCC. Finally, Fig. 1(d) displays a complete hull with the exception of anodes as Variation-3.

(a) Base Case (b) Variation-1 (c) Variation-2 (d) Variation-3

Fig. 1. Different models of the DTMB (Roddier et al., 2009 and Finnigan and Roddier, 2007).

3.2. Numerical model

In this numerical simulation, the chosen numerical model for testing is the DTMB at the scale of 1:22.3 (Variation-2), which was previously tested by Finnigan and Roddier (2007) and Roddier et al., 2009. Hence, the scaled model of the MCC has a diameter of 1.75 m and a draft of 2.95 m. These measurements correspond to a prototype diameter of 39 m and a draft of 65.8 m. The MCC's hull in this study is equipped with strakes, specifically a 3-strake plate with a height equal to 13% of the MCC's diameter. All the CFD cases simulated in this study were performed using the CFD method with STAR-CCM+ software. For the FSI in this numerical research, the LES and VOF methods were utilised by Zhang and Ishihara, (2018 and 2020). According to Fig. 2, the flowchart shows how to model the architecture of numerical models from the first step until the conclusion and post-processing of the Star CCM+ outputs. As seen in Fig. 3, four spring dampers were utilised to present the catenary moorings of the structure. The dimensions and properties of the DTMB of the scaled model and the characteristics of different environmental conditions used in numerical modelling are outlined in Table 1 and Table 2, respectively (Finnigan and Roddier, 2007; Roddier et al., 2009; Lefevre et al., 2012).

Also, the coordinates of the regions and all the MCCs are stated in Table 3. As can be seen in Table 3, the coordinates of all MCCs are at the origin of the CFD coordinates.

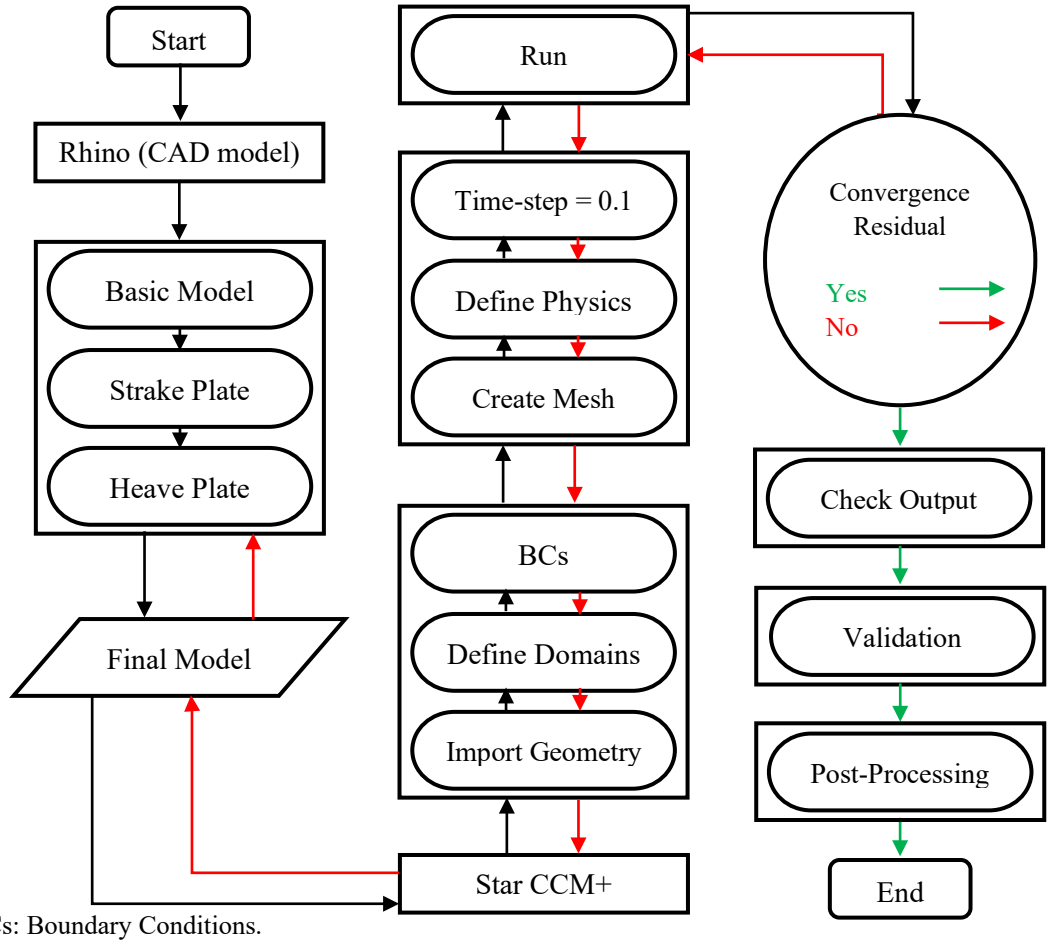

BCs: Boundary Conditions.

Fig. 2. The flowchart of the numerical modeling.

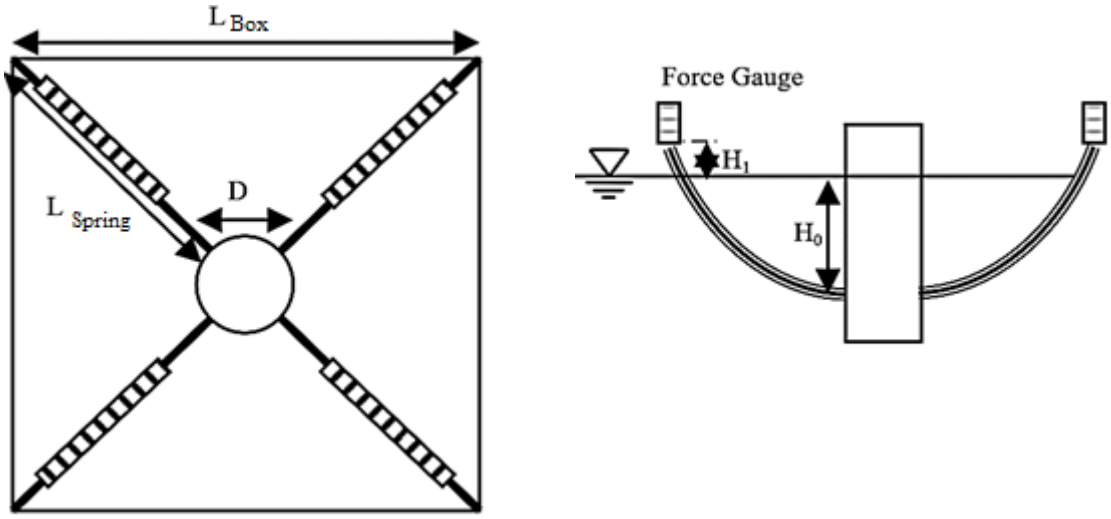

(a) Top View (b) Side View

Fig. 3. Spring system for the scaled model (Finnigan and Roddier, 2007 and Roddier et al., 2009).

Table 1. Structural parameters of the model (Finnigan and Roddier, 2007 and Roddier et al., 2009).

Parameter	Symbol	Unit	Value
MCC's diameter	D_{MCC}	m	1.75
MCC's draft	d	m	2.95
Mass	M	kg	7088.1
Damping ratio	η	%	1.10
Critical damping	C_o	kg/s	255.2
Scale ratio	S_R	-	1:22.3
Stiffness	K	N/m	2111.3
Damping	B	kg/s	2.8
Box Length	L_{Box}	m	14.71
Spring length	L_{Spring}	m	9.15
Ring Draft	H_0	m	1.77
Force Gauge height	H_1	m	0.91

Table 2. Characteristics of different environmental conditions used in numerical modeling.

Condition	Parameter	Symbol	Unit	Value
Marine Current	Reduced velocity	V_R	-	9.0
	Heading	-	degree	0.0
Regular Wave	Wave height	H	m	1.0
	Wave length	L	m	6.0

Table 3. Characteristics of the defined parts in the CFD model.

Parts	Coordinate (m)		Length (m)	Width (m)	Depth of water (m)	Height of air (m)
	1st point	2nd point				
Domain	(-15,-15,-9.7)	(30,15,9.7)	45	30	9.7	9.7
Overlap	(-6.0,-6.0,-6.5)	(20,6.0,6.5)	26	12	6.5	6.5
Overset	(-4.0,-3.0,-4.0)	(8.0, 3.0,4.0)	12	6.0	4.0	4.0
MCCs	(0,0,0)		1.75	1.75	2.95	-

Based on Table 4, in this numerical modeling, seven models have been modeled on Rhino software and then imported into Star CCM+. These models focus on adding the circular heave plate at the keel of the straked MCC, with different diameters from $1.2D_{MCC}$ to $1.6D_{MCC}$. The objective of this research was to analyze and determine the impact of the heave plate diameters on the amplitude of the transitional motions of the straked MCC under marine current and regular waves (Gonçalves et al. 2020, 2022, and 2023) . As shown in Fig. 4, this numerical modeling includes three strakes with an angle of 120 degrees around the MCC, and the heave plate is located at the keel of the MCC (Thiagarajan et al., 2005; Halkyard et al., 2005 and 2006; Lefevre et al., 2012). Due to Fig. 5, the boundary conditions for all CFD simulations are defined as a velocity inlet condition is applied at the fluid domain inlet, a pressure outlet condition is defined at the domain outlet, symmetric boundary conditions are applied to both the lateral sides and top of the domain and the bottom and the MCCs are defined as the wall (Finnigan and Roddier, 2007; Roddier et al., 2009; Lefevre et al., 2012; Kharazmi and Ketabdari, 2022; Li et al., 2023).

Table 4. The configurations of the numerical models.

Name	Configuration	Description
Model A	Bare MCC	D_{MCC}= 1.75 m and d_{MCC}= 2.95m
Model B	Straked MCC	N= 3, θ= 120º, H_S= 0.13D_{MCC}, and γ= 0.5d_{MCC}

Model C	Straked MCC + Heave Plate	N= 3, θ= 120º, H_S= 0.13D_{MCC}, D_{HP}= 1.2D_{MCC}, t_{HP}= 0.1D_{MCC}, and γ= 0.5d_{MCC}
Model D	Straked MCC + Heave Plate	N= 3, θ= 120º, H_S= 0.13D_{MCC}, D_{HP}= 1.3D_{MCC}, t_{HP}= 0.1D_{MCC}, and γ= 0.5d_{MCC}
Model E	Straked MCC + Heave Plate	N= 3, θ= 120º, H_S= 0.13D_{MCC}, D_{HP}= 1.4D_{MCC}, t_{HP}= 0.1D_{MCC}, and γ= 0.5d_{MCC}
Model F	Straked MCC + Heave Plate	N= 3, θ= 120º, H_S= 0.13D_{MCC}, D_{HP}= 1.5D_{MCC}, t_{HP}= 0.1D_{MCC}, and γ= 0.5d_{MCC}
Model G	Straked MCC + Heave Plate	N= 3, θ= 120º, H_S= 0.13D_{MCC}, D_{HP}= 1.6D_{MCC}, t_{HP}= 0.1D_{MCC}, and γ= 0.5d_{MCC}

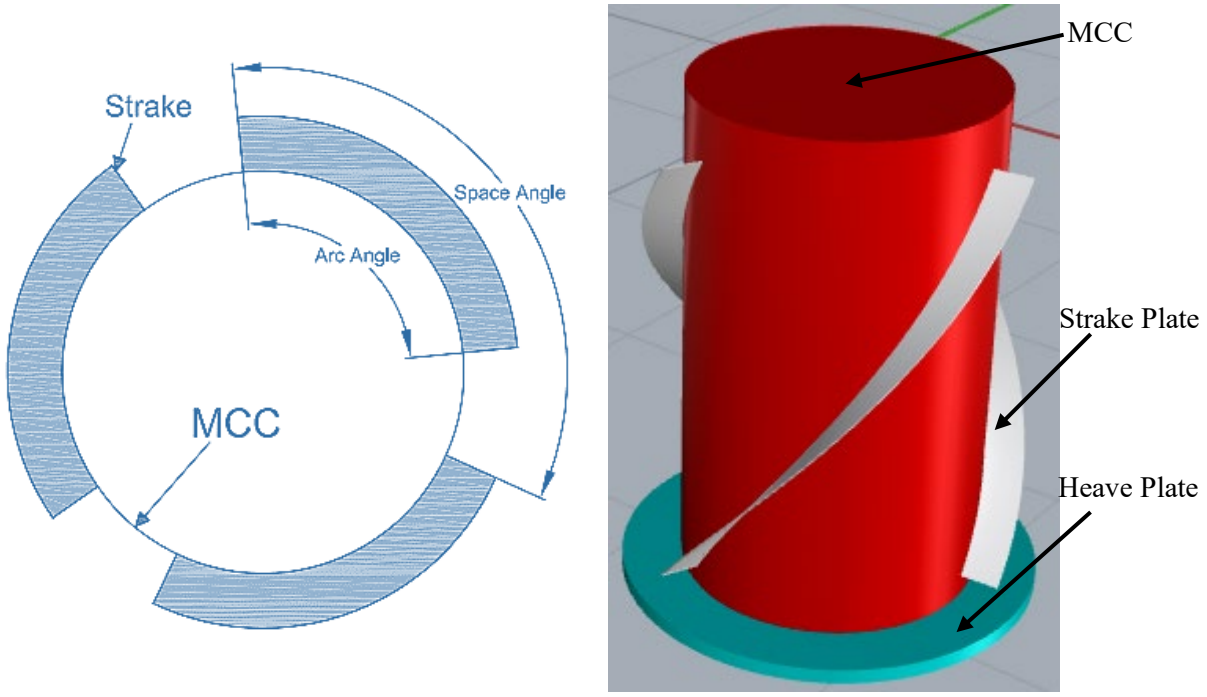

(a) Straked MCC (top view) (b) Straked MCC + Heave Plate (3D view)

Fig. 4. The MCC with strake and heave plate.

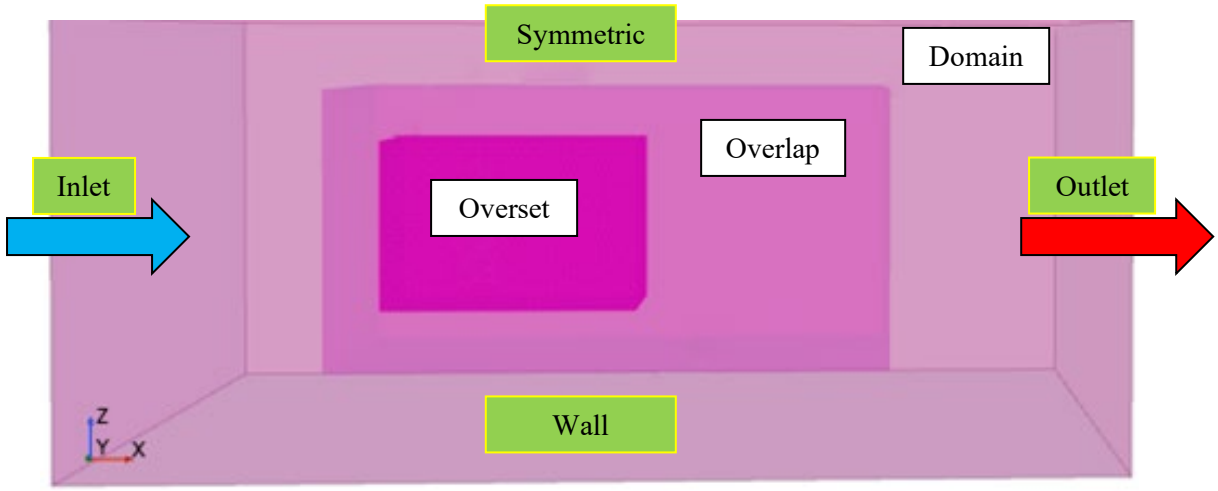

Fig. 5. The boundary conditions in the CFD simulation (Side view).

In this study, five different mesh types, namely very fine mesh, fine mesh, base mesh, medium mesh, and coarse mesh, were utilized to show the mesh independence of the meshing process in the CFD. Table 5 illustrates the quantity of the total cells in the CFD's mesh. Based on the

data presented in Table 5, after analyzing the maximum amplitude of the sway motion (A) per MCC's diameter (Max A/D_{MCC}), it was found that the very fine mesh, fine mesh, base mesh, medium mesh, and coarse mesh have the differences of 9.65%, 9.80%, 10%, 13%, and 19.5%, respectively under the marine current with reduced velocity (V_R) of 8 and velocity inlet of 0.853 m/s (U_C=0.853 m/s). As can be seen in Fig. 6(a), due to the small difference in the accuracy of the result of very fine mesh and fine mesh with the base mesh, and also to reduce the computational cost in the process of numerical analysis which is illustrated in Fig. 6(b), the base mesh was chosen in the CFD simulation. Hence, the sizes of the base mesh for all regions and MCCs with different heave plate diameters are given in Table 6 (Lefevre et al., 2012, Kharazmi and Ketabdari, 2022). In addition, the base mesh configuration in different areas, such as Domain, Overlap, and Overset is depicted in Fig. 7. Moreover, the base mesh around the MCC and the arrangement of the strake plates due to the marine and wave directions is illustrated in Fig. 8.

Table 5. Mesh independency in the CFD's simulation.

Type	**Total cells**	**Max A/D_{MCC}**	**Error (%)**
Very Fine Mesh	24×10^6	0.333	9.65
Fine Mesh	16×10^6	0.334	9.80
Base Mesh	8×10^6	0.335	10.00
Medium Mesh	6×10^6	0.345	13.00
Coarse Mesh	4×10^6	0.367	19.50

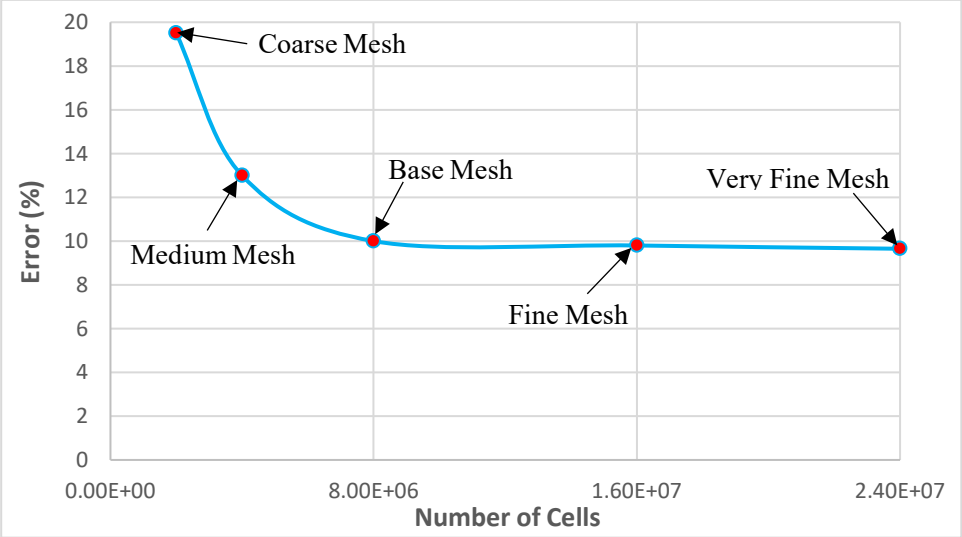

(a) Percentage of error

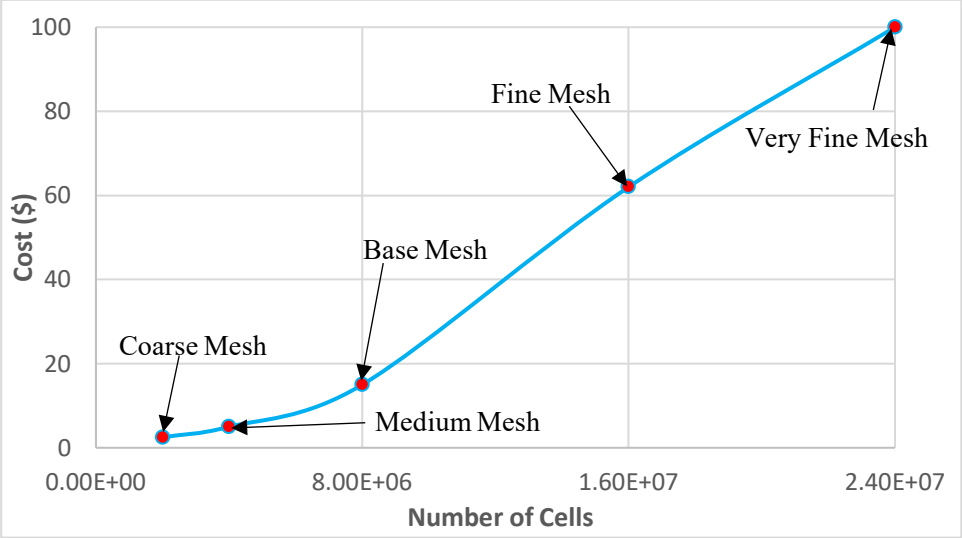

(b) Computational cost of completed run

Fig. 6. Comparison of error percentage and computational cost in defined meshes under V_R=8.

Table 6. Size of the base mesh of the regions and parts in the CFD.

Part	Size (m)		
	Minimum	**Target**	**Maximum**
Domain region	0.5	0.5	0.5
Overlap region	0.25	0.25	0.25
Overset region	0.0625	0.0625	0.0625
Bare MCC	0.0625	0.0625	0.0625
Bare MCC + Strake	0.015625	0.015625	0.015625
Straked MCC + Heave plate	0.015625	0.015625	0.015625

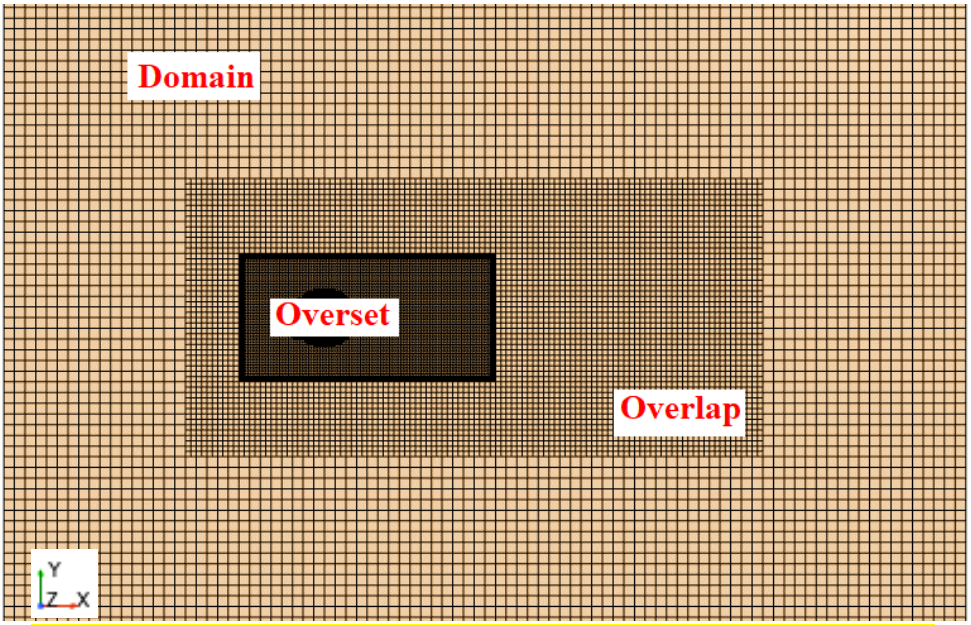

Fig. 7. The base mesh in the different regions of the CFD method (top view).

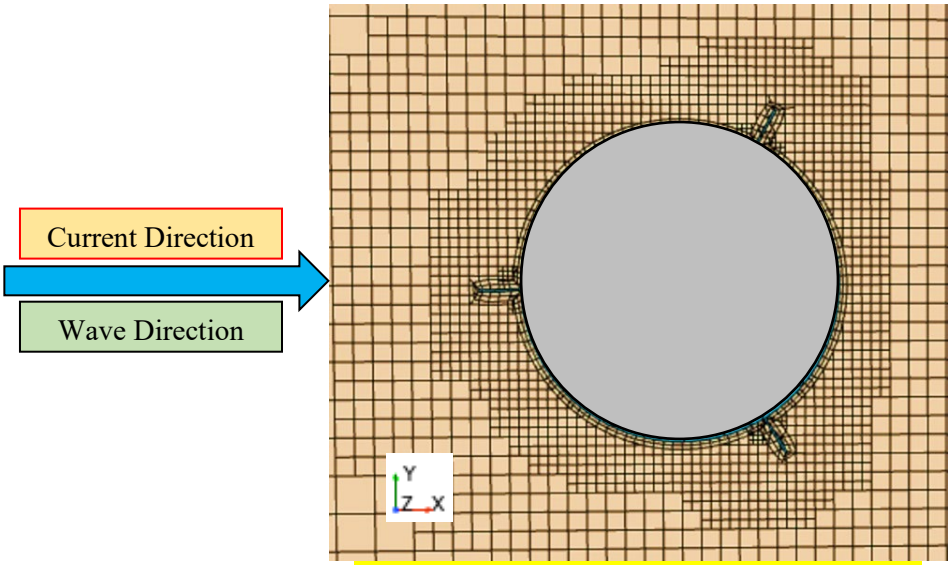

Fig. 8. The base mesh near the MCC (top view).

The Overset mesh was established for this computational configuration. This type of meshing is utilized to divide a computational domain into multiple meshes that overlap each other in an arbitrary manner. It is most efficient for problems involving large movements and optimization studies where the geometry can be enclosed within an Overset region and positioned differently. The Overset mesh approach connects regions by exchanging data between acceptor cells in one region and specially marked active cells (donor cells) in another region. A typical Overset simulation consists of a Domain region that envelops the entire solution domain and an Overset region that surrounds the MCC. The outer surface of the Overset region is defined as an Overset boundary. To connect these two regions (Domain and Overset), STAR-CCM+ employs a hole-cutting process, marking cells in the Domain region inactive if their solution solely comes from the Overset region. Within both Domain and Overset regions, several layers of overlapping cells participate in the data exchange process. The solution is computed simultaneously for all active cells in all regions, meaning the meshes are implicitly coupled.

When referring to the value of a variable in an acceptor cell from one region, a combination of variable values at donor cells from another region is used to provide the value. This value is directly reflected in the coefficient matrix of the equation system. This tight coupling between the Domain and Overset regions allows for a solution with minimal iteration errors. The convergence rate of the iterative solution method is, therefore, similar to that of a single mesh with the same resolution. For all cases, the Y+ value was maintained between 0 and 30 in the extruded mesh near the wall surfaces. Extruded mesh layers were employed to capture the boundary layer around the MCC. The hybrid wall treatment, known as the "All Y+" treatment, was used to smoothly blend a low Re wall treatment with a high Re wall function. Five different mesh resolutions were employed: coarse, base, medium, fine, and very fine meshes. Due to the results in Fig. 6, the base model exhibits good convergence and was selected for this computational setup (Wang et al., 2010; Lefevre et al., 2012; CD-adapco, 2013; Kharazmi and Ketabdari, 2022).

Hence, checking the validity and quality of the CFD's mesh, there are several factors to consider. These factors include Chevron quality, Cell quality, Face validity, and Skewness angle, which are illustrated in Fig. 9(a)~(d). Due to Fig. 9(a), the Chevron quality refers to the arrangement of cells in the CFD's mesh. It determines how well the cells are aligned and connected to each other. A zero Chevron quality means that the cells are well-aligned and connected in the CFD's mesh, the zero Chevron quality resulting in a more accurate representation of the flow in the simulation. As can be seen in Fig. 9(b), the Cell quality is a measure of the shape and size of each individual cell in the CFD's mesh. Ideally, the Cell quality should be one, the lowest value in this numerical calculation is equal to 0.35, which is an acceptable value for CFD's mesh. Face validity indicates how well the faces of adjacent cells in the mesh are connected to each other. The faces should be properly aligned and should not have any overlaps or gaps by adjusting this value by one, which is displayed in Fig. 9(c). Based on Fig. 9(d), the Skewness angle measures the distortion or deviation from perfect orthogonality between the faces of adjacent cells. Lower Skewness angles indicate better quality, as they represent a more orthogonal or perpendicular arrangement of faces in the mesh. The maximum acceptable value of the Skewness angle is 85, and the maximum value of this factor in this CFD's mesh is 70 (CD-adapco, 2013).

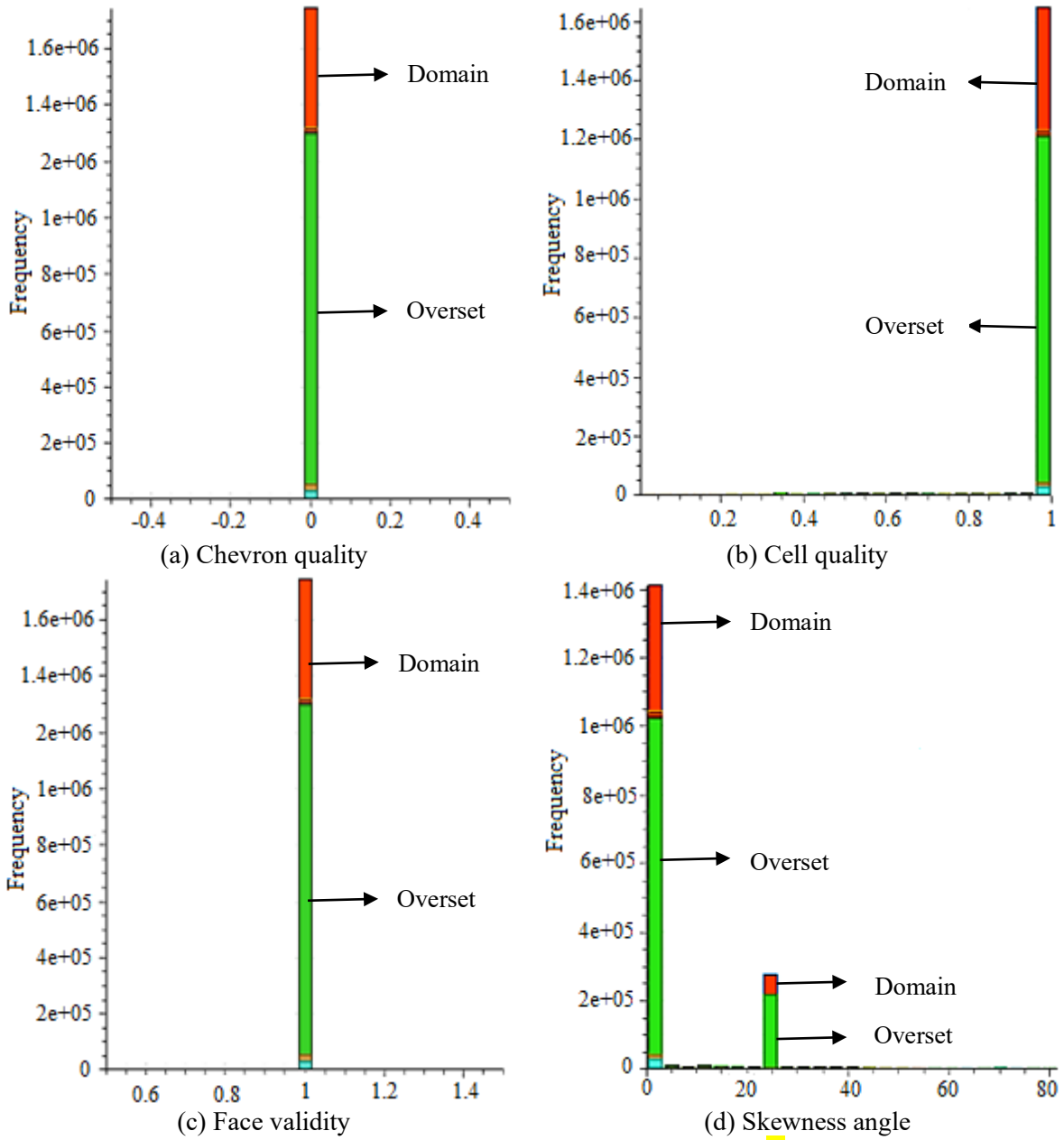

Fig. 9. Checking the validity and quality of the CFD's mesh.

3.3. Validation

3.3.1. Reduced Velocity (V_R)

The numerical results obtained in this study were validated against the experimental data obtained in a previous study (Finnigan and Roddier, 2007 and Roddier et al., 2009), ensuring the accuracy and reliability of the computational model. Based on Table 7 for the 3-straked MCC was simulated under different reduced velocities (V_R), while other parameters, such as mesh size, boundary conditions, and time steps were constant (Van Dijk et al., 2003). Due to Fig. 10, the present model was validated in the experimental tests under different values of V_R in the sway motion by the maximum amplitude of the sway motion (A) per the MCC's diameter (D_{MCC}) at different values of V_R. As can be seen in Table 8, the maximum and minimum errors have occurred at the V_R of 7 and 9. To evaluate the amplitude of the transitional motions of the

straked MCC with different configurations of heave plates, the reduced velocity of 9 was chosen in the marine current condition. The error values in this present work might be due to the different placement of the strakes around the MCC due to the experimental and numerical research (Finnigan and Roddier, 2007; Roddier et al., 2009; and Kharazmi and Ketabdari, 2022).

Table 7. The characteristics of the marine currents (Lefevre et al., 2012).

Reduced velocity (-)	Froude number (-)	Re number (-)	Inlet velocity (m/s)
5.0	0.13	8.6e+05	0.56
6.0	0.15	1.0e+06	0.64
7.0	0.18	1.2e+06	0.746
8.0	0.21	1.4e+06	0.853
9.0	0.23	1.5e+06	0.9593

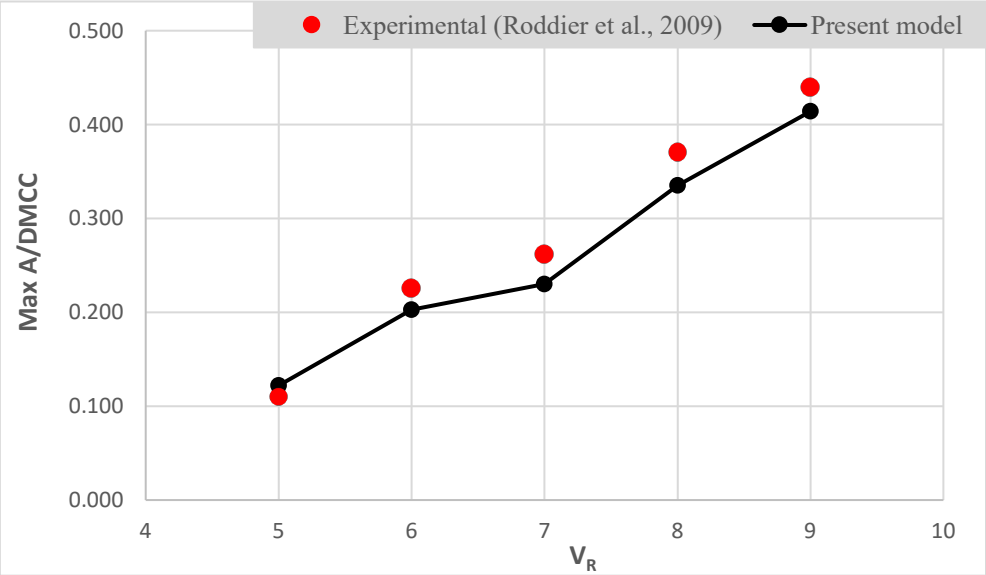

Fig. 10. The validation of the present model for the experimental test under marine current.

Table 8. The error values under different reduced velocities (V_R).

Reduced velocity (V_R)	Experimental (Roddier et al., 2009)	Present model	Error (%)
5	0.110	0.122	-11
6	0.226	0.203	10
7	0.262	0.230	12
8	0.370	0.335	10
9	0.440	0.414	6

3.3.2. Natural period

In this research, the results from both approaches showed that the platform with the heave plate experienced lower heave motion due to induced damping and added mass coefficients in the governing equation. Hence, in the FDT of this research, the initial vertical displacement was obtained by specifying the initial velocity of $V_0 = -1$ m/s in each direction (Ciba, 2021 and Ciba et al.. Based on Roddier et al., (2009), due to the similarity between the spring systems and models, the natural periods of surge and sway align effectively. As can be seen in Fig. 11, the FDT of the bare MCC, 3-straked MCC, and 3-straked MCC+ heave plate with a diameter of

$1.4D_{MCC}$ under the transitional motions was done. Hence, including the heave plate at the keel of the straked MCC decreased the amplitude of the transitional motions, which is more noticeable in the heave motion. This reduction is attributed to the introduction of the added mass and damping coefficients into the dynamic equations. Due to Takata et al., (2022), the results showed that incorporating heave plates led to an increase in natural periods compared to the bare MCC. The inclusion of heave plates decreased the amplitude by around 15-25% and 45-55% in the surge/sway and heave motions, respectively. The natural periods of the structure, as determined by the FDT, are stated in Table 9 (Ali et al., 2021; Murdjito et al., 2021; Ciba et al., 2022). Based on Fig. 12, the difference in natural period between the experimental and numerical results for the surge and sway motion is 1.2%.

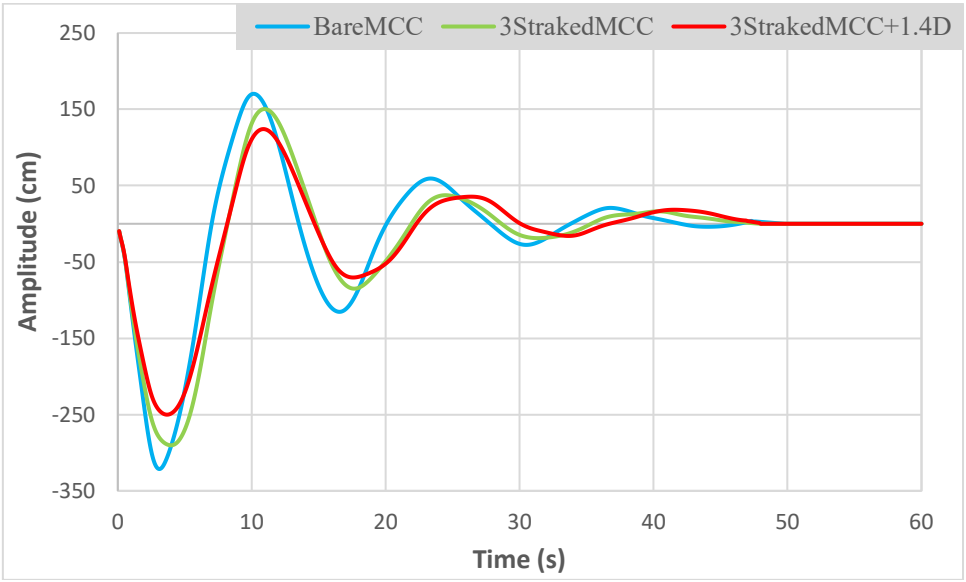

(a) Surge and Sway motion

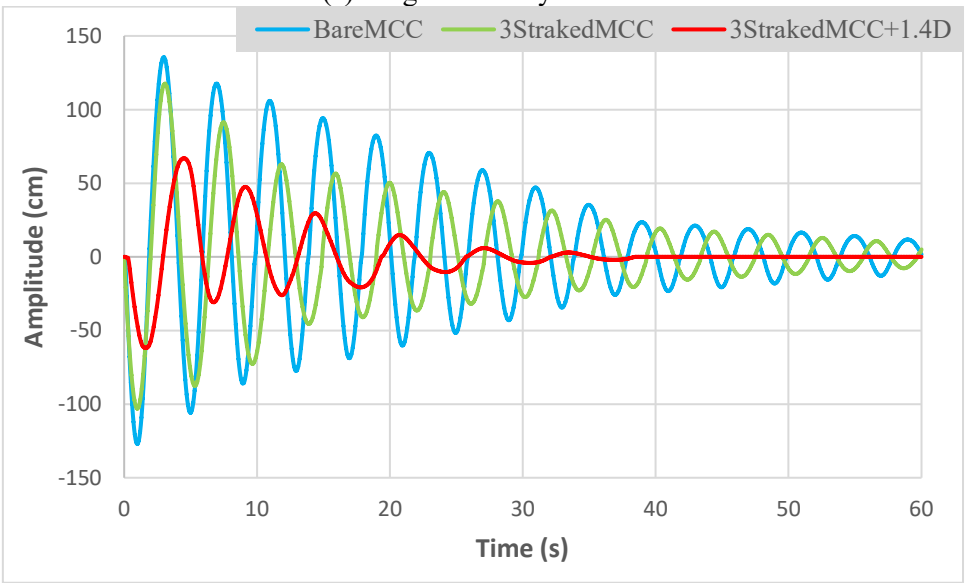

(b) Heave motion

Fig. 11. The results of the FDT with the initial velocity.

Table 9. The natural period of the models.

Motion	Model	Natural period (s)	
		Experimental (Roddier et al., 2009).	Numerical

Surge and Sway	Bare MCC	-	12.50
	3-Straked MCC	16.40	16.60
	3-Straked MCC+1.4D	-	17.00
Heave	Bare MCC	-	4.00
	3-Straked MCC	-	4.30
	3-Straked MCC+1.4D	-	6.35

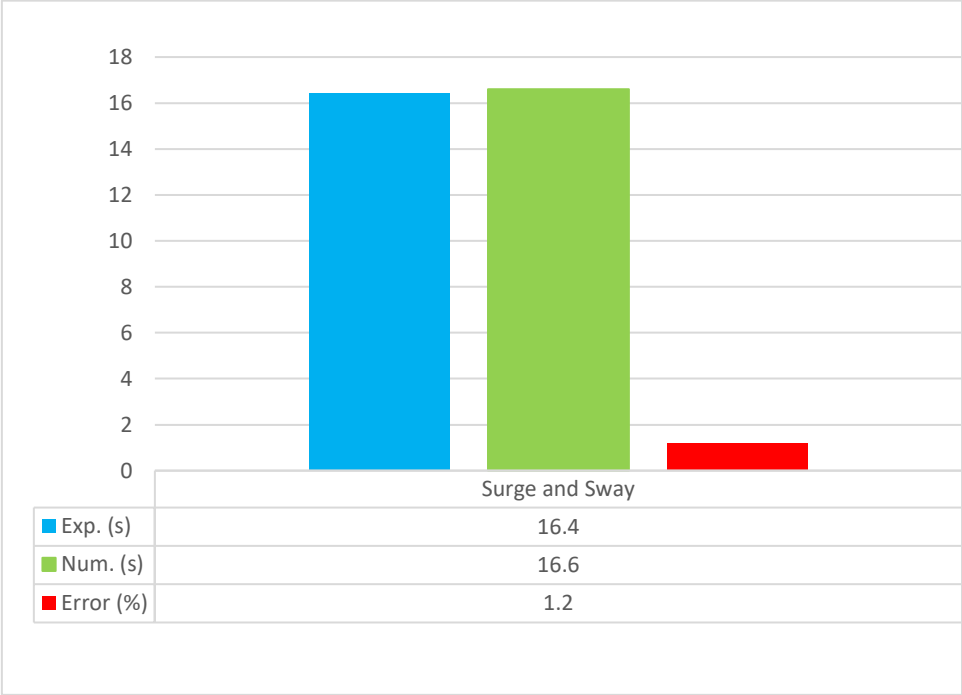

Fig. 12. The results of natural period of the present model and experimental of Roddier et al., (2009).

4. Numerical results

4.1. Marine current

In order to investigate the numerical models under the marine current due to experimental tests (Finnigan and Roddier, 2007, Roddier et al., 2009, and Lefevre et al., 2012), we employed a marine current with a V_R of 9. Subsequently, we analysed the amplitude of the transitional motions of surge, sway, and heave in the models, which can be found in Table 4.

4.1.1. Surge motion

As can be seen in Fig. 13(a), the results of the surge motion demonstrate that the presence of a strake plate has reduced the surge motion in comparison to the bare MCC. Additionally, due to Fig. 13(b)~(f), the inclusion of a heave plate located at the keel of the straked MCC has noticeably decreased the surge motion. Based on the numerical models described in Table 4, it can be concluded that heave plates with diameters ranging from $1.3D_{MCC}$ to $1.4D_{MCC}$ have acceptable performance in reducing the surge's amplitude. Based on Fig. 13(a)~(f), the 3-straked MCC+ heave plate with a diameter of $1.4D_{MCC}$ showed the most effective performance in reducing the surge's amplitude of the structure.

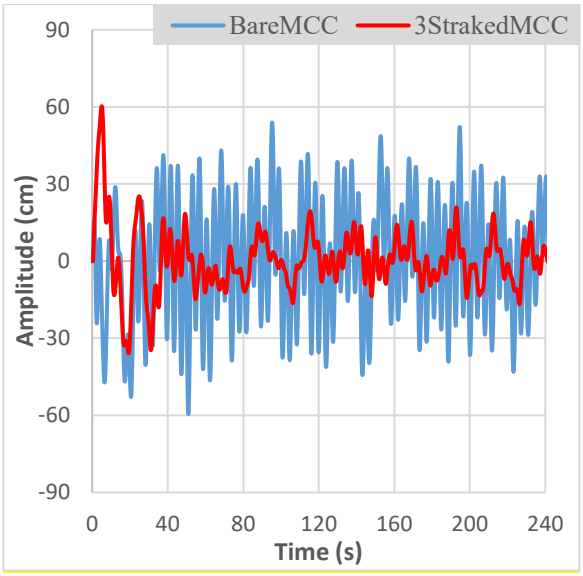

(a) Bare MCC and 3-Straked MCC

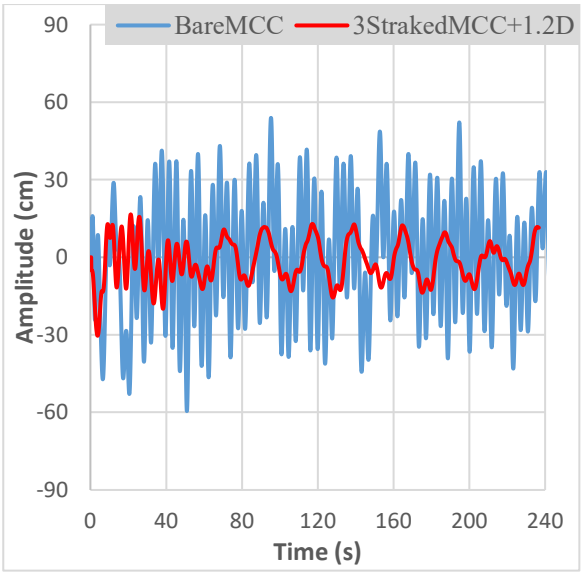

(b) Bare MCC and 3-Straked MCC+1.2D_{MCC}

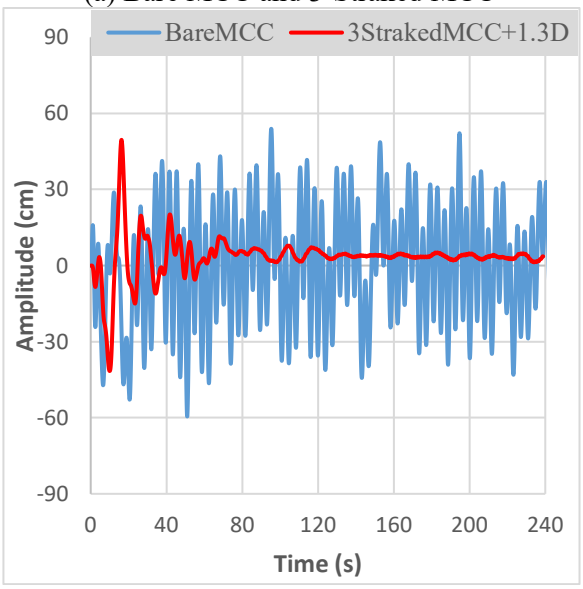

(c) Bare MCC and 3-Straked MCC+1.3D_{MCC}

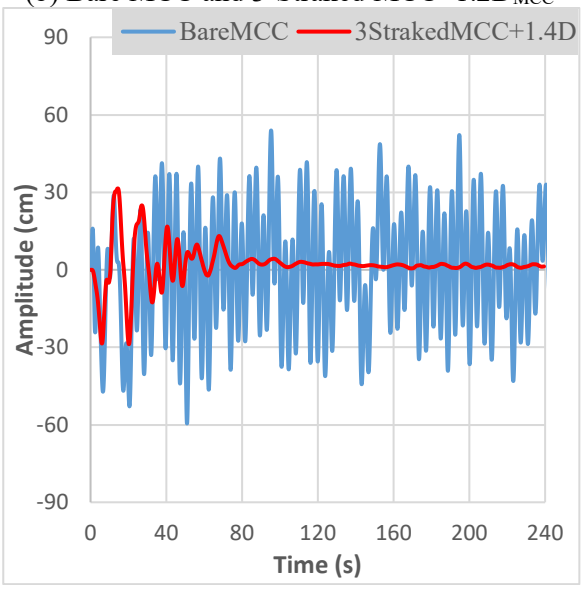

(d) Bare MCC and 3-Straked MCC+1.4D_{MCC}

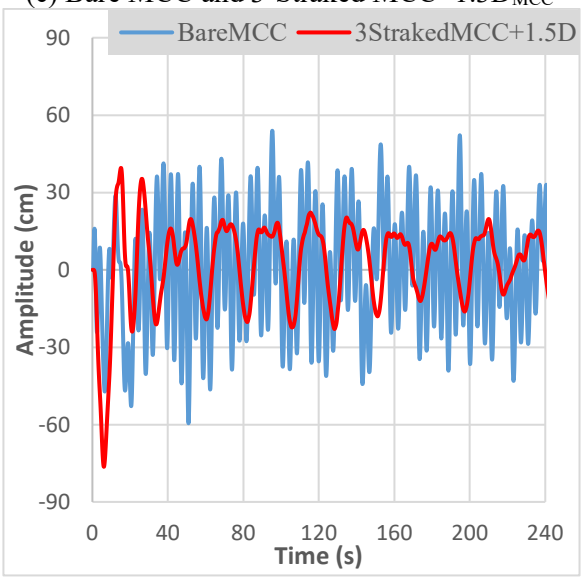

(e) Bare MCC and 3-Straked MCC+1.5D_{MCC}

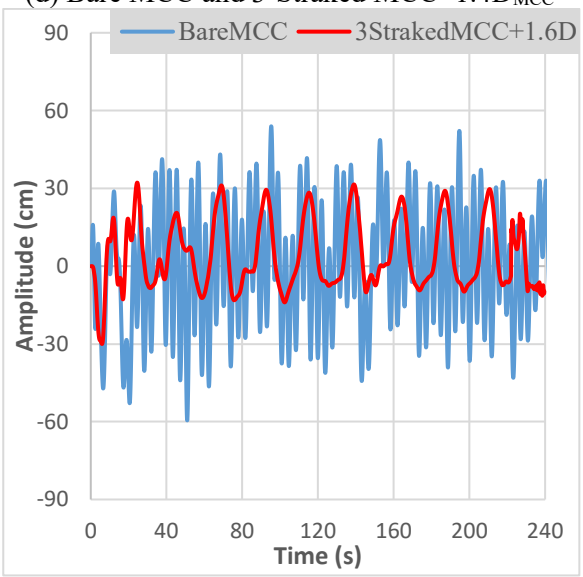

(f) Bare MCC and 3-Straked MCC+1.6D_{MCC}

Fig. 13. The results of the surge motion under the marine current.

4.1.2. Sway motion

The findings shown in Fig. 14(a)~(f) indicated that the strake plate and heave plate have lowered the amplitude of the sway motion compared to the bare MCC. Furthermore, the numerical outcomes showed that the inclusion of a heave plate positioned at the keel of the MCC has reduced the sway motion's amplitude. According to the numerical models presented in Table 4, it can be inferred that models of 3-straked MCC+1.2D_{MCC}, 3-straked MCC+1.4D_{MCC}, and 3-straked MCC+1.5D_{MCC}, provided acceptable results in reducing the sway's amplitude of the structure. The most effective performance in decreasing the amplitude of the sway motion under marine current with a V_R of 9 is 3-straked MCC+ heave plate with a diameter of 1.4D_{MCC}, as can be observed in Fig. 14(d).

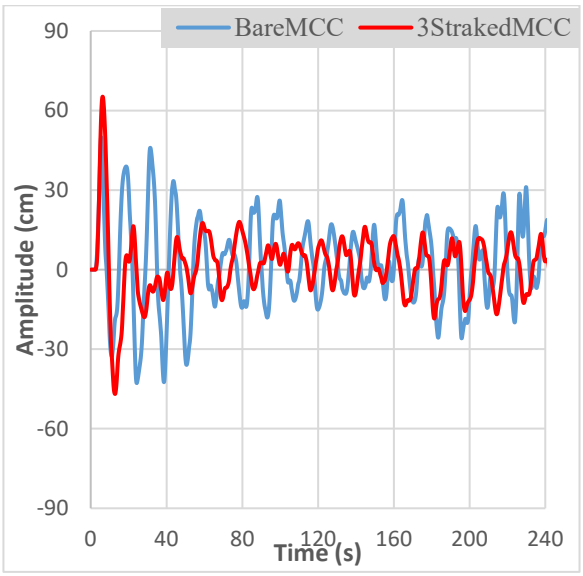

(a) Bare MCC and 3-Straked MCC

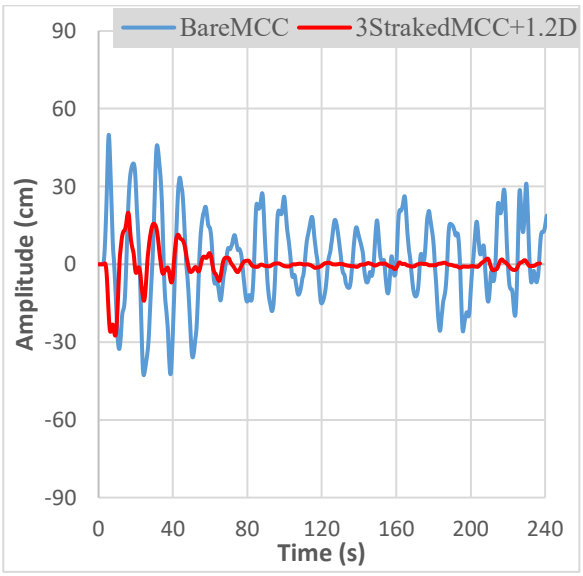

(b) Bare MCC and 3-Straked MCC+1.2D_{MCC}

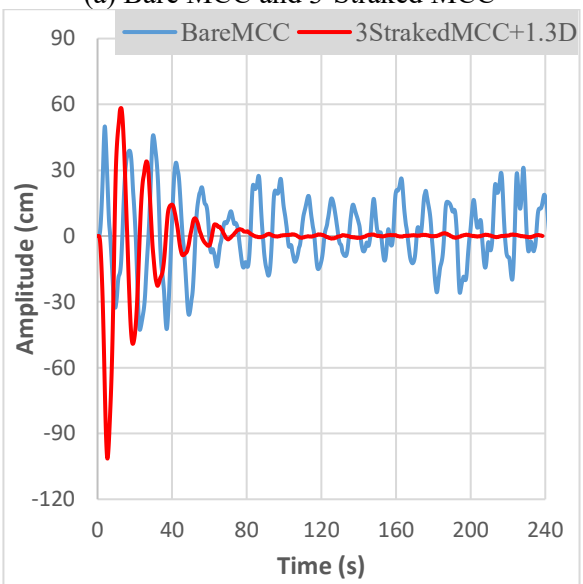

(c) Bare MCC and 3-Straked MCC+1.3D_{MCC}

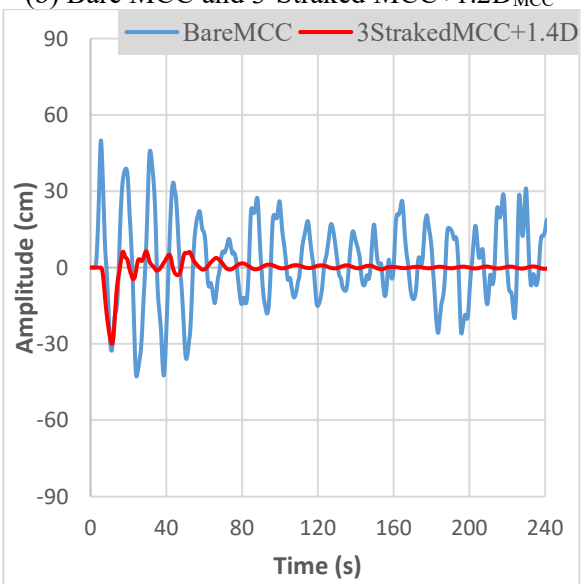

(d) Bare MCC and 3-Straked MCC+1.4D_{MCC}

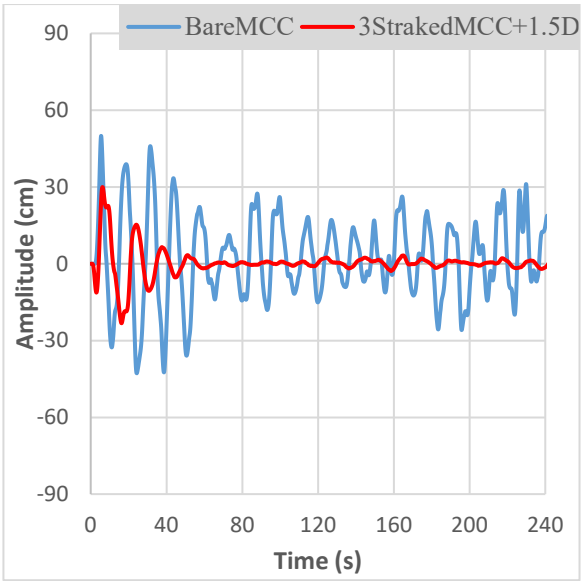

(e) Bare MCC and 3-Straked MCC+1.5D_{MCC}

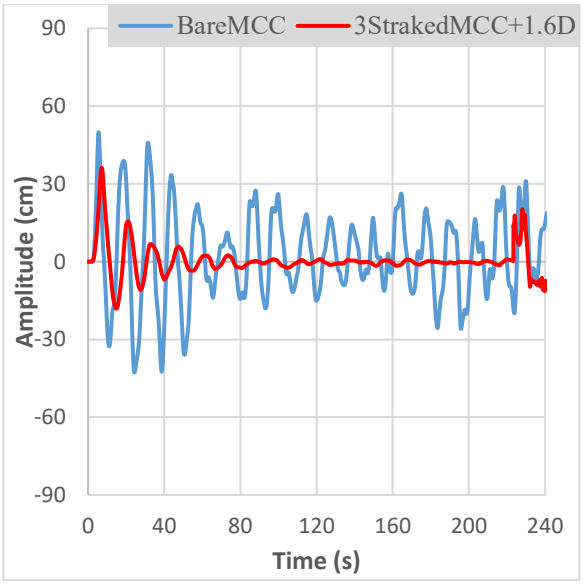

(f) Bare MCC and 3-Straked MCC+1.6D_{MCC}

Fig. 14. The results of the sway motion under the marine current.

4.1.3. Heave motion

As shown in Fig. 15(a), the presence of a strake plate has decreased the amplitude of the heave motion in comparison to the bare MCC. Moreover, incorporating the heave plate with a different diameter at the keel of the 3-straked MCC greatly reduced the heave motion's amplitude, as evident in Fig. 15(b)~(f). Referring to the numerical models specified in Table 4, it is observed that models D and E, where the diameter of the heave plate ranges from 1.3D_{MCC} to 1.4D_{MCC}, represent superior performance in decreasing the amplitude of the heave motion of the structure. Due to the results, the 3-straked MCC+ heave plate with 1.4D_{MCC} has the best behavior in decreasing the heave motion's amplitude of the straked MCC.

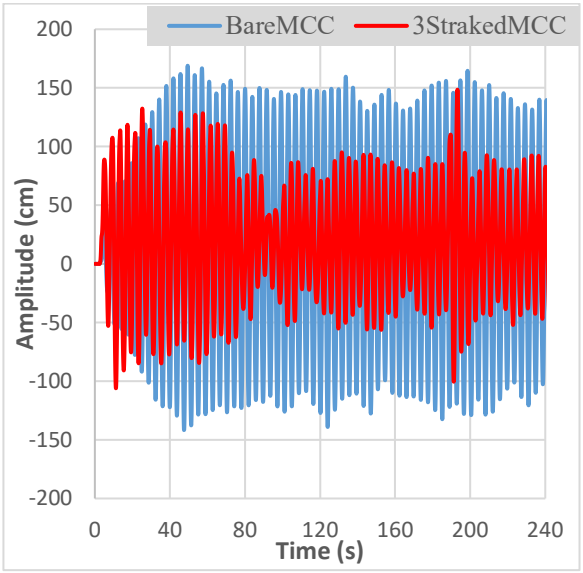

(a) Bare MCC and 3-Straked MCC

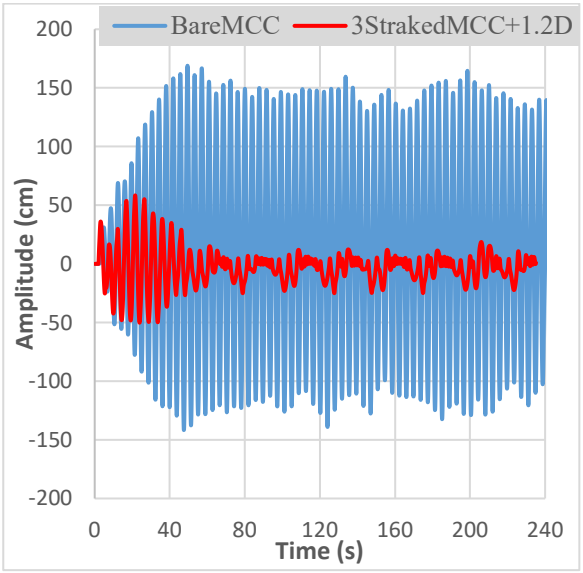

(b) Bare MCC and 3-Straked MCC+1.2D_{MCC}

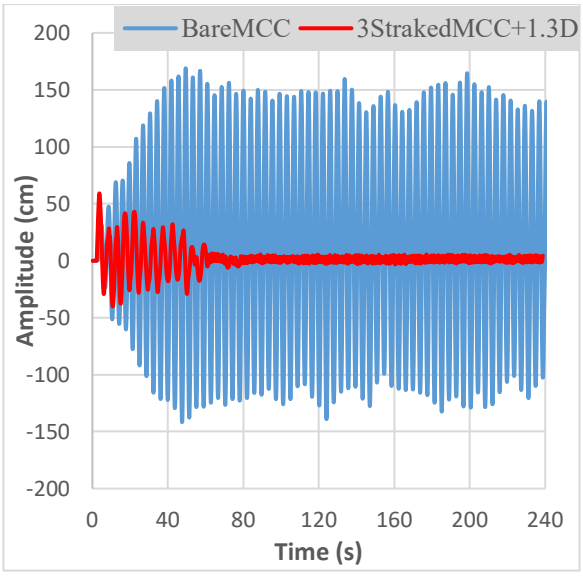

(c) Bare MCC and 3-Straked MCC+1.3D_{MCC}

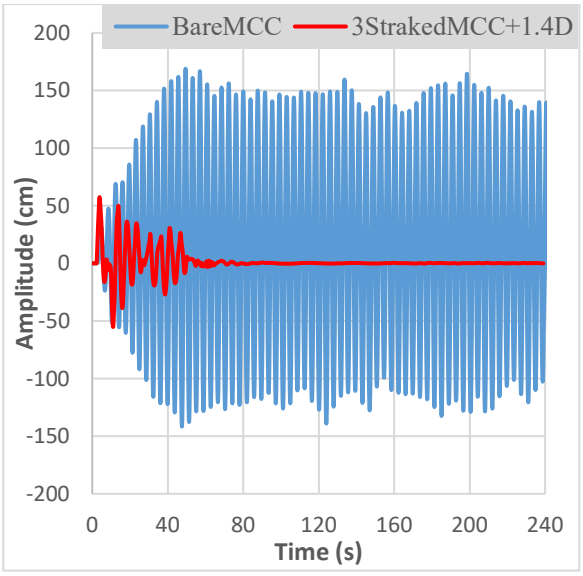

(d) Bare MCC and 3-Straked MCC+1.4D_{MCC}

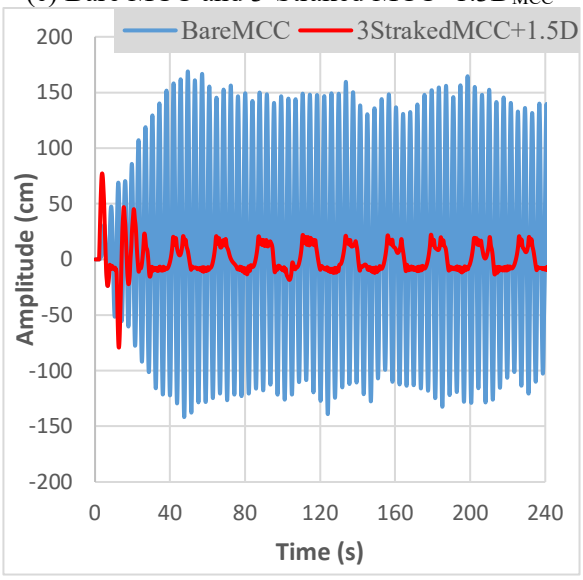

(e) Bare MCC and 3-Straked MCC+1.5D_{MCC}

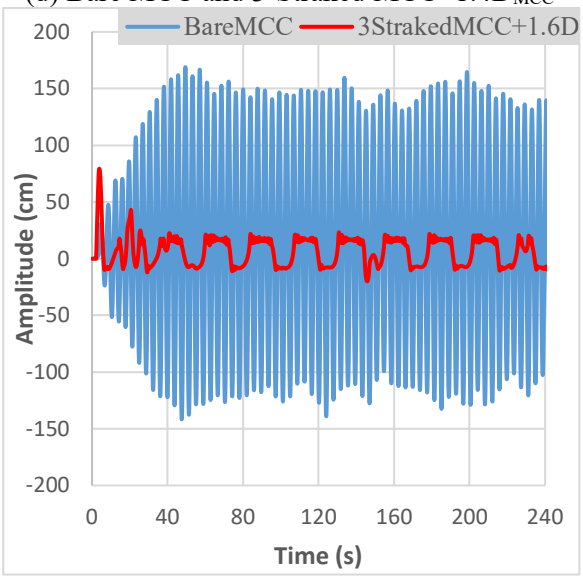

(f) Bare MCC and 3-Straked MCC+1.6D_{MCC}

Fig. 15. The results of the heave motion under the marine current.

4.2. Regular waves

To examine the different configurations of the MCC under the waves, which are listed in Table 4. We utilised regular waves with a 0.5-meter amplitude and a 6-meter wavelength to evaluate the amplitude of the transitional motions of surge, sway, and heave of the models under regular waves.

4.2.1. Surge motion

Fig. 16(a) clearly shows that the surge motion is decreased when a strake plate is utilized compared to the bare MCC. Furthermore, based on Fig. 16(b)~(f), the addition of a heave plate positioned at the keel of the MCC helped the strake plates reduce the amplitude of the surge

motion. The results revealed that the 3-straked MCC+ heave plate with 1.3D_{MCC} demonstrated the most effective model in reducing the amplitude of the surge motion under the regular waves.

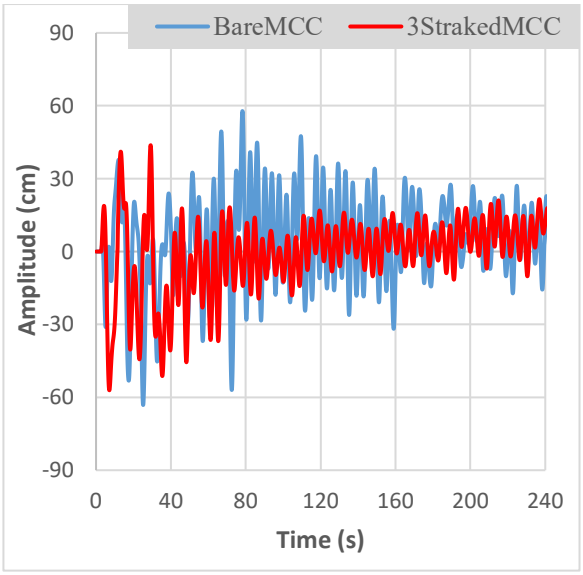

(a) Bare MCC and 3-Straked MCC

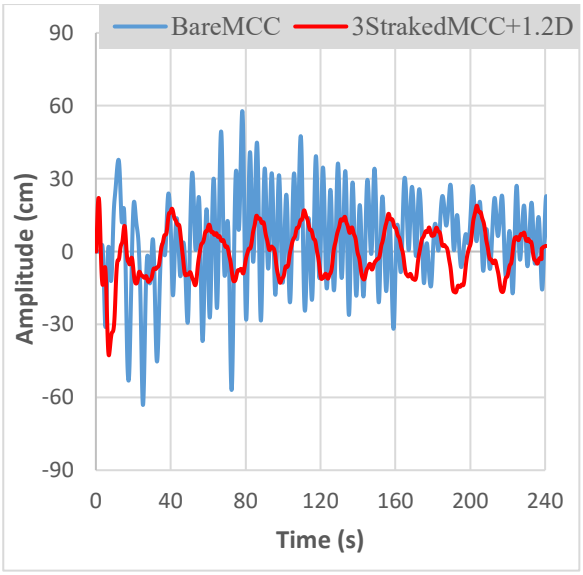

(b) Bare MCC and 3-Straked MCC+1.2D_{MCC}

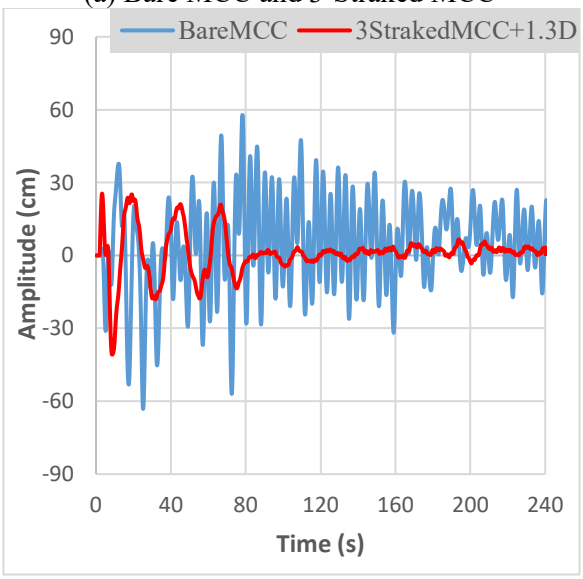

(c) Bare MCC and 3-Straked MCC+1.3D_{MCC}

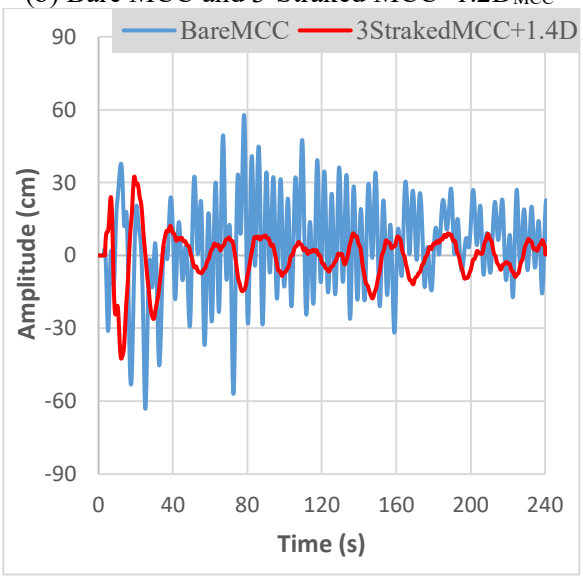

(d) Bare MCC and 3-Straked MCC+1.4D_{MCC}

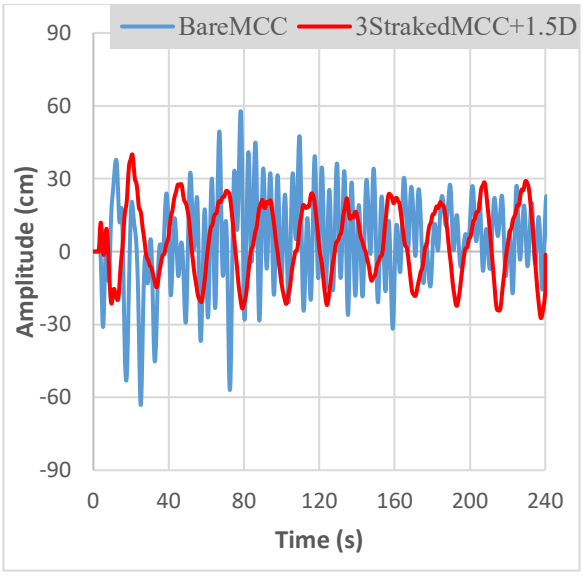

(e) Bare MCC and 3-Straked MCC+1.5D_{MCC}

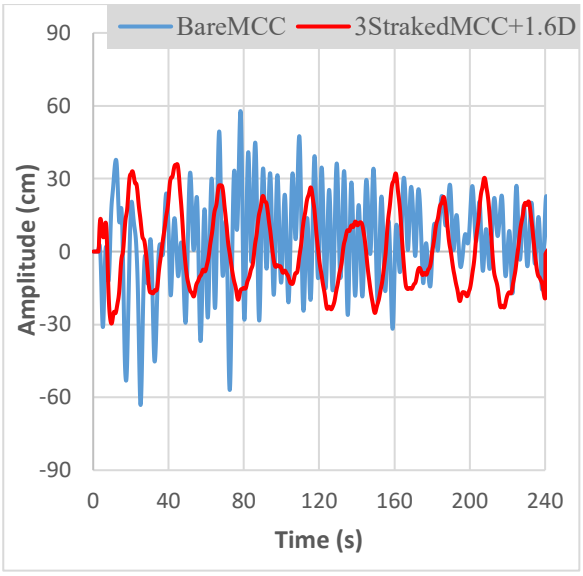

(f) Bare MCC and 3-Straked MCC+1.6D_{MCC}

Fig. 16. The results of the surge motion under the regular waves.

4.2.2. Sway motion

The results depicted in Fig. 17(a) demonstrated that the utilization of a strake plate has decreased the sway motion compared to the bare MCC. As can be seen in Fig. 17(b)~(f), the numerical findings indicated that the incorporation of the heave plate with an optimal diameter, where placed at the keel of the MCC has significantly helped the strake plates in reducing the amplitude of the sway motion. Therefore, the 3-straked MCC+ heave plate with a diameter of 1.4D_{MCC} yielded the most favourable outcomes in reducing the sway amplitude of the structure when subjected to regular waves.

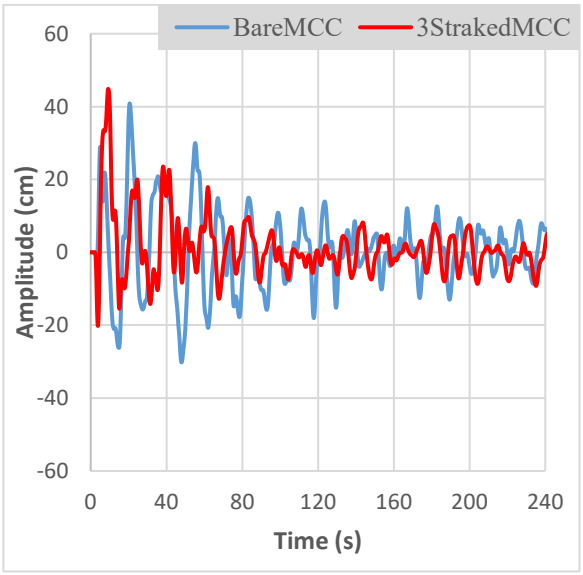

(a) Bare MCC and 3-Straked MCC

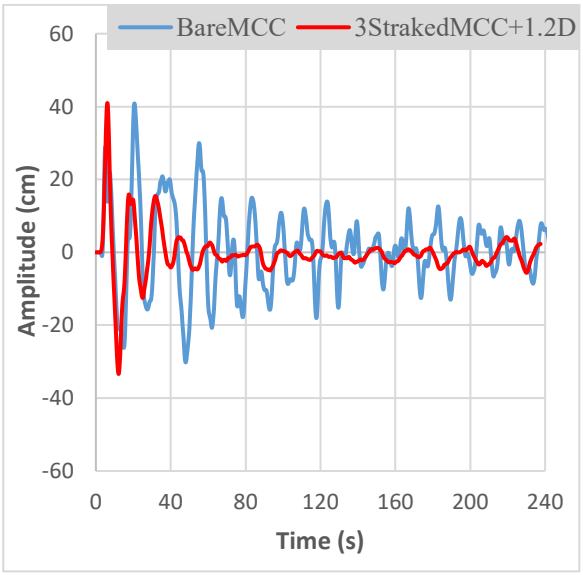

(b) Bare MCC and 3-Straked MCC+1.2D_{MCC}

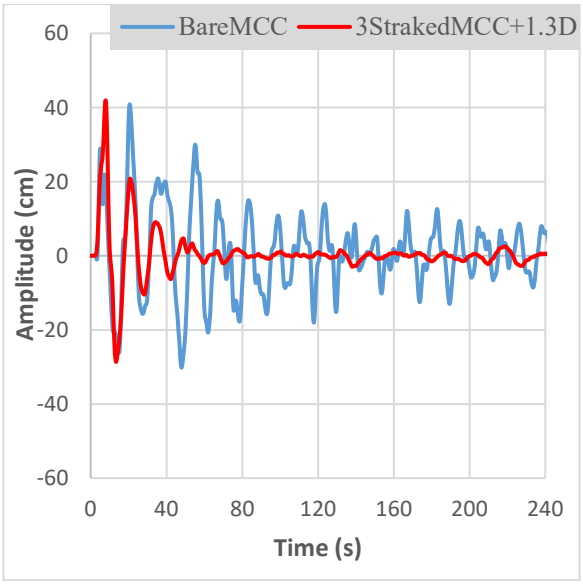

(c) Bare MCC and 3-Straked MCC+1.3D_{MCC}

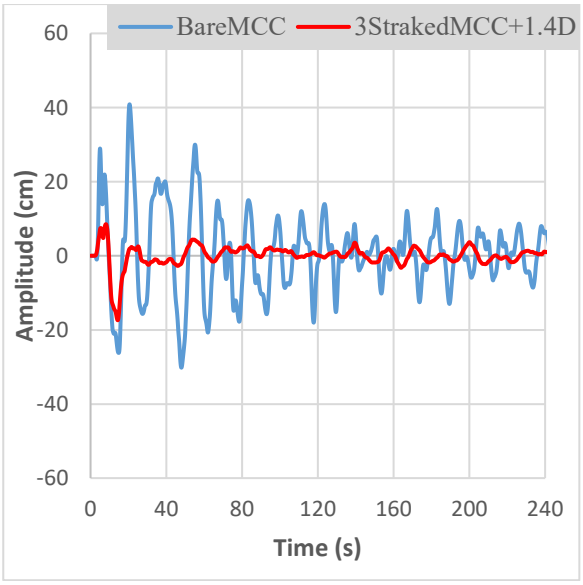

(d) Bare MCC and 3-Straked MCC+1.4D_{MCC}

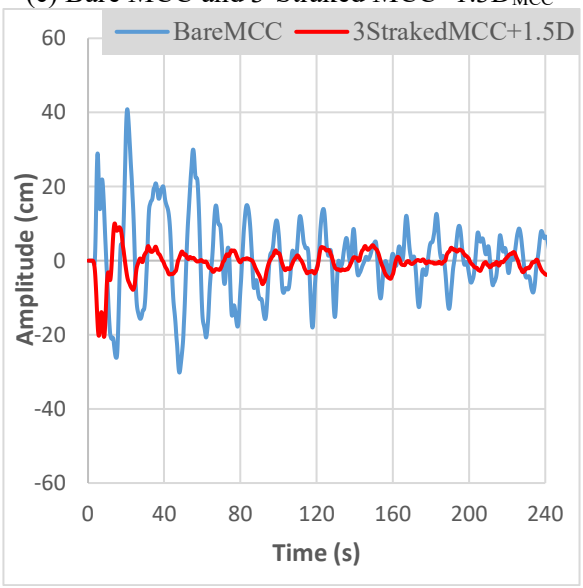

(e) Bare MCC and 3-Straked MCC+1.5D_{MCC}

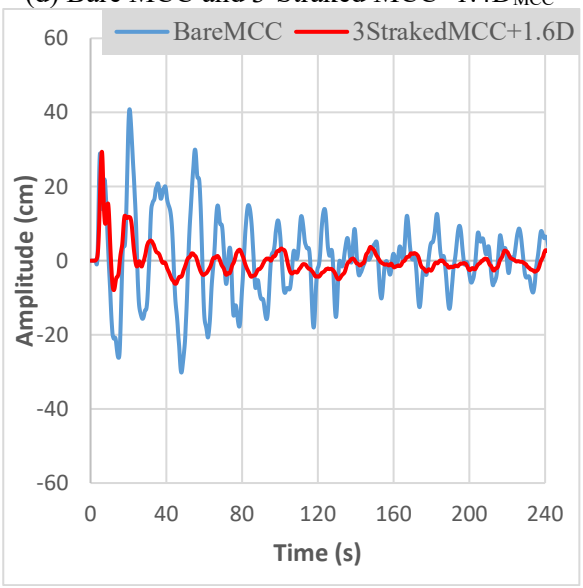

(f) Bare MCC and 3-Straked MCC+1.6D_{MCC}

Fig. 17. The results of the sway motion under the regular waves.

4.2.3. Heave motion

The presence of a strake plate had an effect on reducing the heave motion's amplitude of the 3-straked MCC compared to the bare MCC, which is illustrated in Fig. 18(a). By using the heave plate with different diameters at the keel of the MCC, there was a significant reduction in the amplitude of the heave motion, as shown in Fig. 18(b)~(f). Hence, the 3-straked MCC+ 1.3D_{MCC} has the best performance in reducing the amplitude of the heave motion of the straked MCC under regular waves.

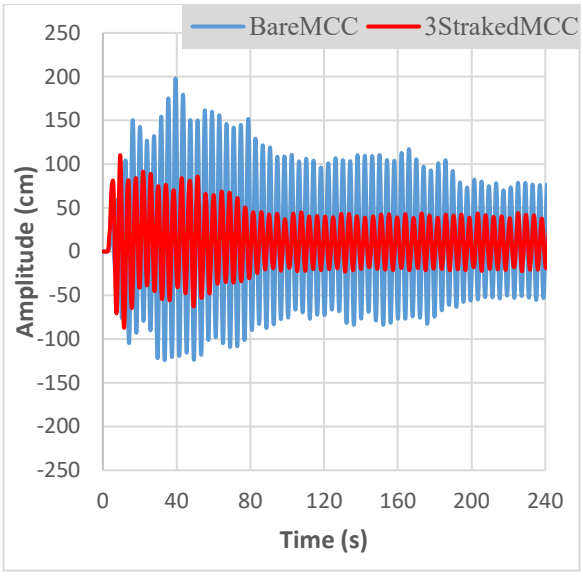

(a) Bare MCC and 3-Straked MCC

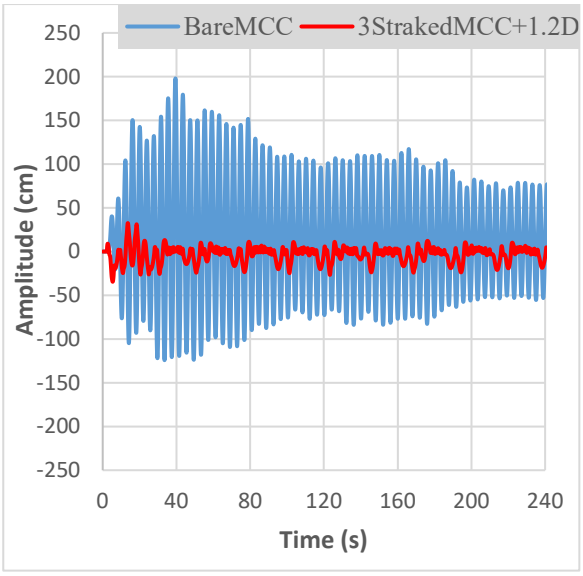

(b) Bare MCC and 3-Straked MCC+1.2D_{MCC}

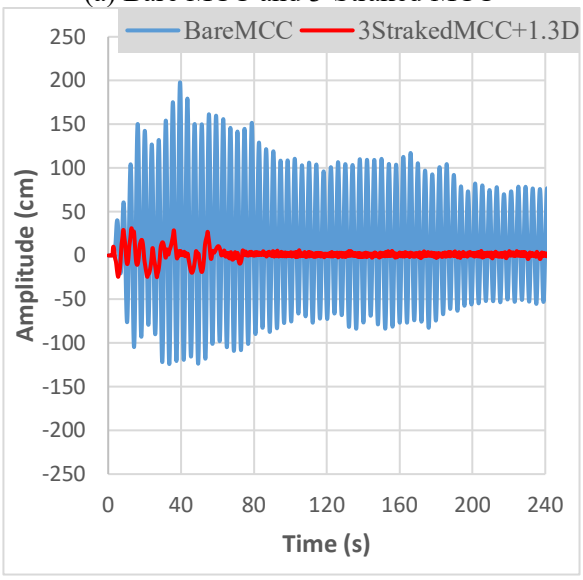

(c) Bare MCC and 3-Straked MCC+1.3D_{MCC}

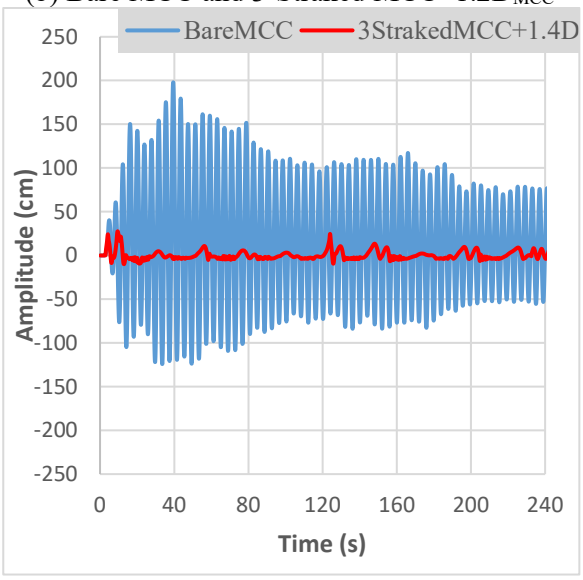

(d) Bare MCC and 3-Straked MCC+1.4D_{MCC}

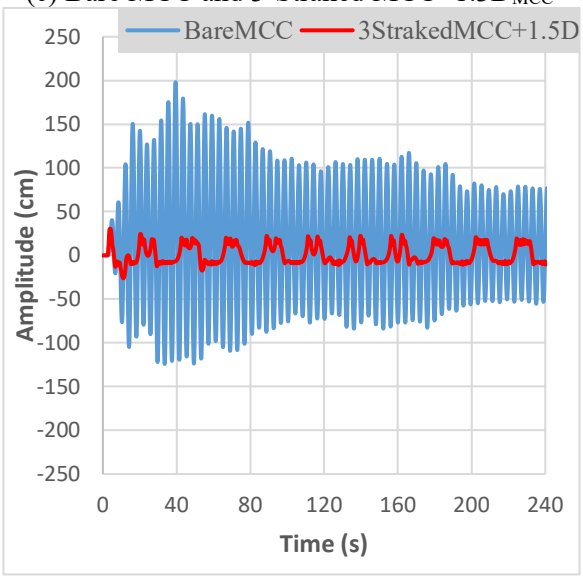

(e) Bare MCC and 3-Straked MCC+1.5D_{MCC}

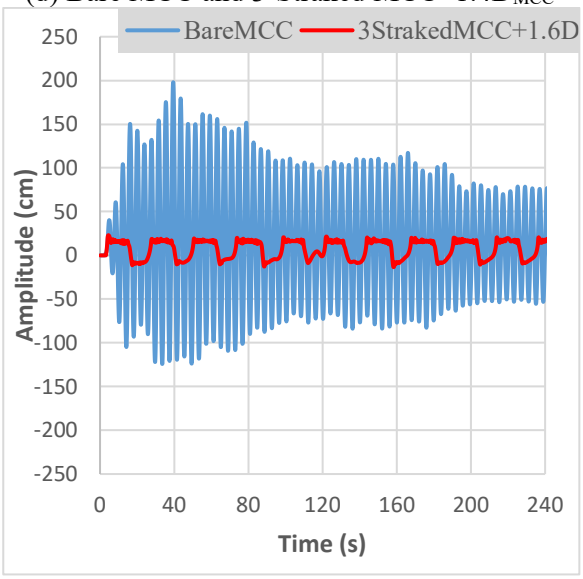

(f) Bare MCC and 3-Straked MCC+1.6D_{MCC}

Fig. 18. The results of the heave motion under the regular waves.

4.3. Summary of the transitional motions

The optimal configuration for both marine current and regular waves models can be found in Table 10. Based on the information provided in Table 10, the 3-straked MCC + heave plate with a diameter of $1.4D_{MCC}$ (model E), demonstrated the most effective performance in reducing the amplitude of surge, sway, and heave motions caused by marine currents. Regarding the regular waves in Table 10, the model D (3-straked MCC+ heave plate with a diameter of $1.3D_{MCC}$) had the best performance in reducing the amplitude of surge and heave motions, while the model E (3-straked MCC+ heave plate with a diameter of $1.4D_{MCC}$) had the best performance in reducing the sway's amplitude of the MCC. In general, it can be concluded that model C, model D, and model E (MCC+3-strake+1.2-$1.4D_{MCC}$) are the most suitable models for reducing the amplitude of the surge, sway, and heave motions of the MCC in the two states of marine current and regular waves.

Table 10. The summary of the current and regular waves in numerical results.

Condition	V_R (-)	U_C (m/s)	Wave		Motion	Model	
			Amplitude (m)	Length (m)		Good	Best
Marine current	9	0.9593	-	-	Surge	C to E	E
Marine current	9	0.9593	-	-	Sway	C to F	E
Marine current	9	0.9593	-	-	Heave	C to E	E
Regular wave	-	-	0.5	6	Surge	C to E	D
Regular wave	-	-	0.5	6	Sway	C to G	D and E
Regular wave	-	-	0.5	6	Heave	C to E	D

4.4. Cross-flow (CF) and In-Line (IL) displacements

According to Table 10, model E (3-satraked MCC+ heave plate with a diameter of $1.4D_{MCC}$) had the best performance in reducing the amplitude of the three transitional motions under the marine current with V_R of 9. Hence, the +CF and +IL displacements of the bare MCC and model E are displayed in Fig. 19. Based on Fig. 19(a)~(b), the utilization of the heave plate and strake plates in the MCC has reduced the amplitude of the CF and IL displacements, while the period of the structure has increased compared to the bare MCC. Also, according to Table 10, it can be inferred that model D (consisting of the 3-straked MCC and heave plate with a diameter of $1.3D_{MCC}$) displayed the most effective performance in reducing the amplitude of the three transitional motions under the regular waves with a 0.5-meter amplitude and a 6-meter wavelength. Consequently, the displacements of +CF and +IL for both the bare MCC and model D will be presented in Fig. 20. According to Fig. 20(a)~(b), the use of the heave plate and strake plates in the MCC has decreased the CF and IL displacements, as well as increased the structure's period compared to the bare MCC.

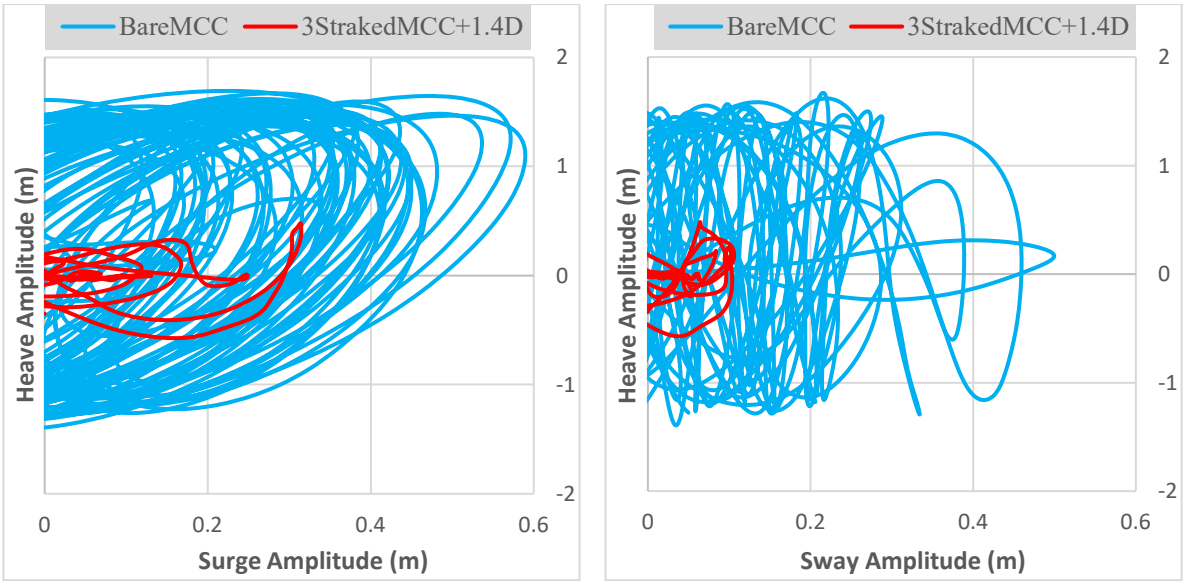

(a) +IL displacement (b) +CF displacement

Fig. 19. The +IL and +CF displacements of the bare MCC and the 3-straked MCC+1.4D_{MCC} under marine current with a V_R=9.

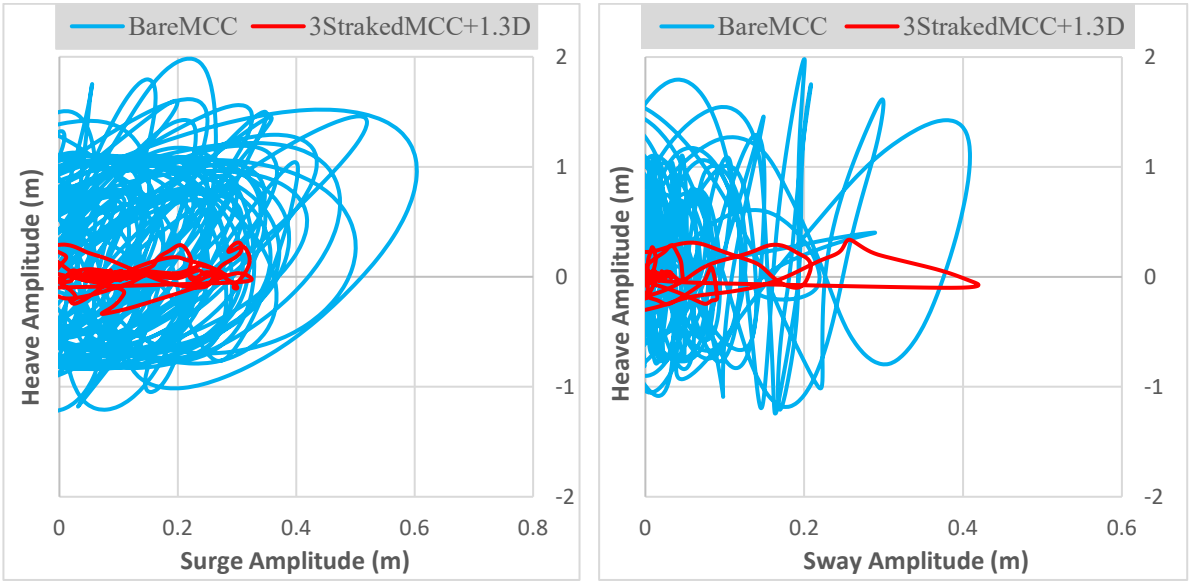

(a) +IL displacement (b) +CF displacement

Fig. 20. The +IL and +CF displacements of the bare MCC and the 3-straked MCC+1.3D_{MCC} under regular waves.

4.5. Von Kármán vortex street

The Von Kármán vortex street is a phenomenon that occurs when fluid flow past a bluff body, such as an MCC. This creates a series of swirling vortices that form in a staggered arrangement downstream of the MCC. These vortices alternate in direction and are shed at a particular frequency. According to the research conducted by (Hwang et al., 2003; Sun et al., 2020; Bandizadeh Sharif et al., 2023), flow-induced vibration (FIV) suppression devices prevent the formation of the Von Kármán vortex street in downstream of the structure. Therefore, Fig. 21 demonstrates the impact of the strake plate on the shear layer of an MCC in the wake at a Re number of 1×10^4. Hence, the illustration in Fig. 21(a)~(b) reveals that the configuration of the strake plates has enlarged the wake's width, leading to the prevention of the Von Kármán vortex

street by eliminating the interference between the two shear layers along the sides of the MCC in the downstream region of the MCC (Banerjee et al. 2021). Based on the latest research (Nguyen et al., 2023; Liu et al., 2023; Yawar et al., 2023; Pang et al., 2023; Yuan et al., 2023), as can be seen in Fig. 21(b), the Von Kármán vortex street has been eliminated in the 3-straked MCC. Due to Fig. 22(a)~(c), the presence of the strake plates has the greatest impact on eliminating this phenomenon, as they cause significant changes in the flow separation angle in the wake layer and prevent the interaction of the shear layers on both sides of the MCC at downstream. Ultimately, this leads to the removal of the Von Kármán vortex street at downstream of the 3-straked MCC. The outcomes of the numerical analysis demonstrated that the presence of the heave plate impacted the suppression of the VIM phenomenon. Also, an increase in the height of the heave plate (referred to as skirt height by Gonçalves et al., 2020) has resulted in a noticeable decrease in the vortex shedding's strength in downstream of the structure. Hence, the effect of a 3-straked MCC+ heave plate with a skirt height is suggested for future work.

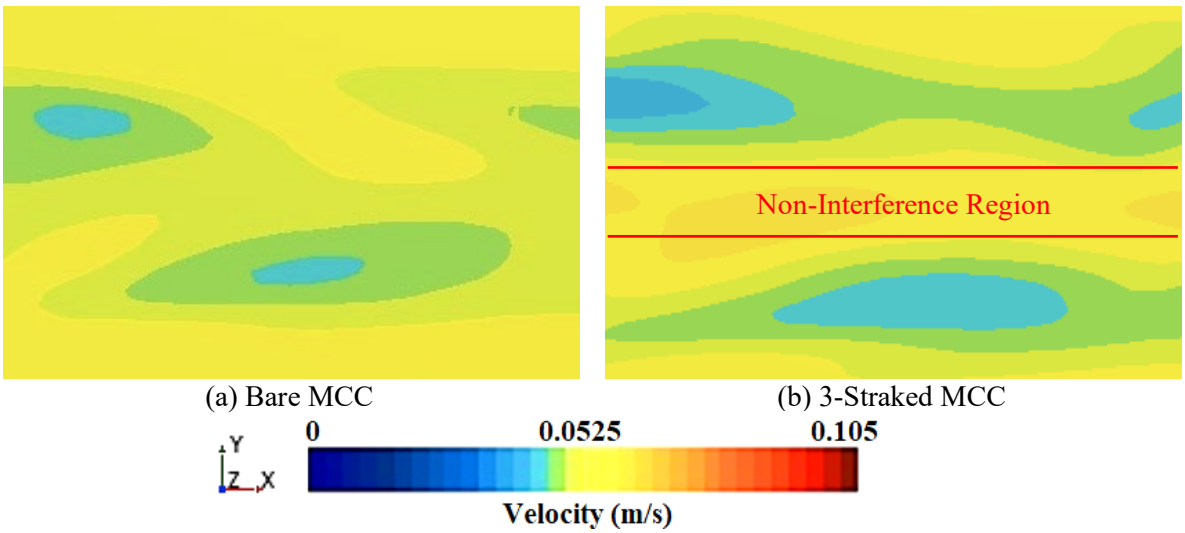

(a) Bare MCC (b) 3-Straked MCC

Fig. 21. The shear layers at downstream of the MCC at the Re number of 1×10^4.

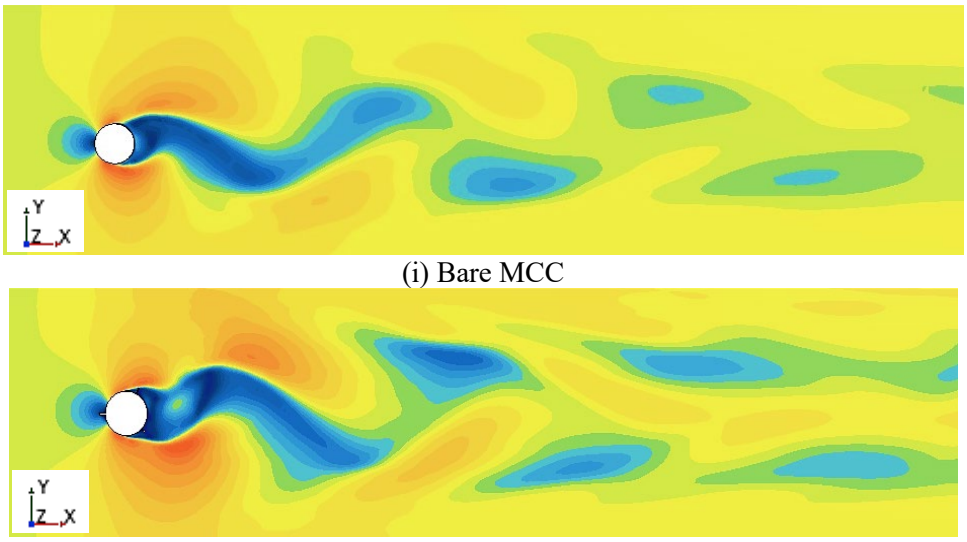

(i) Bare MCC

(ii) 3-Straked MCC

(a) Time = t + (10 × Time step = 0.001)

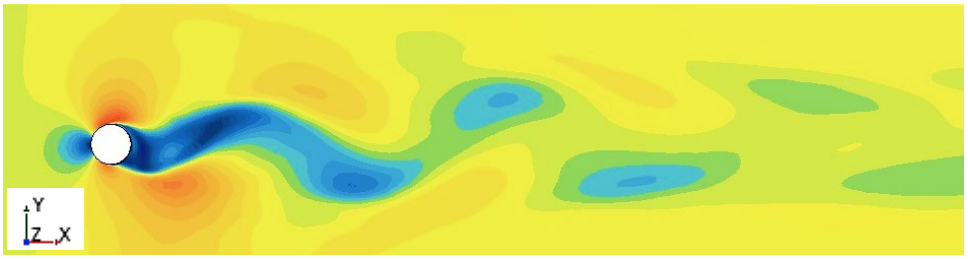

(i) Bare MCC

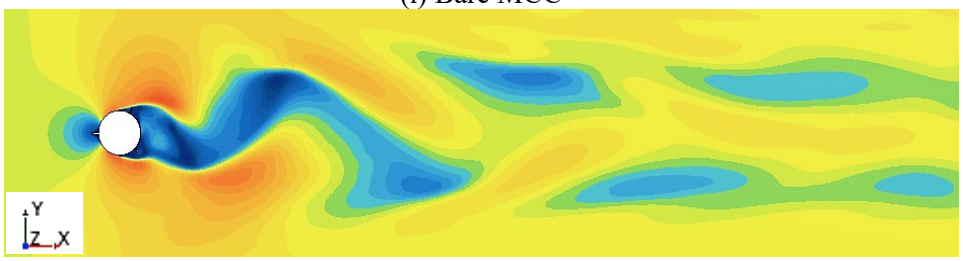

(ii) 3-Straked MCC

(b) Time = t + (20 × Time step = 0.001)

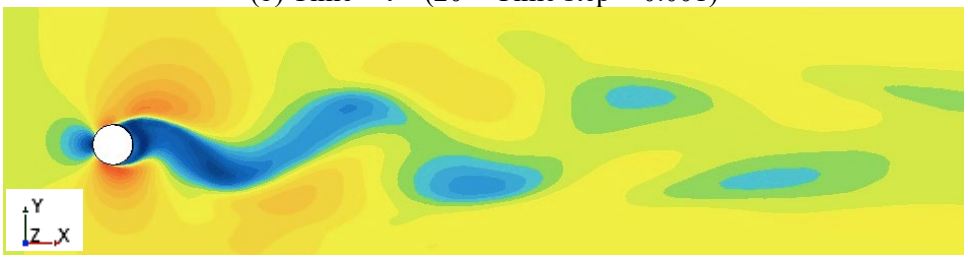

(i) Bare MCC

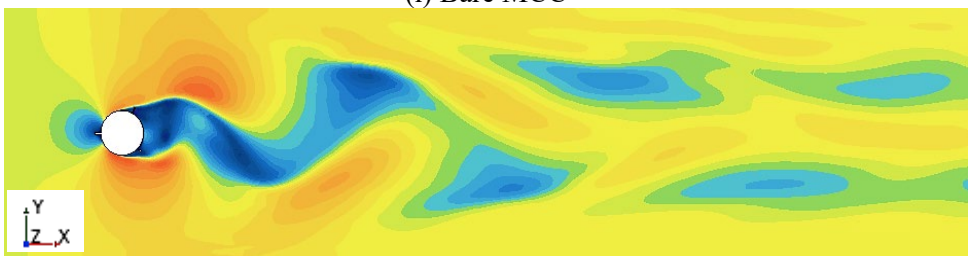

(ii) 3-Straked MCC

(c) Time = t + (30 × Time step = 0.001)

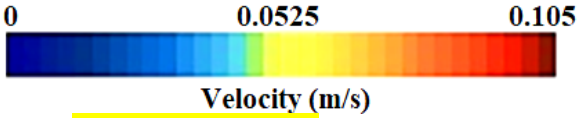

Fig. 22. The flow pattern at the downstream of the MCC under the Re number of 1×10^4.

5. Conclusion

This numerical study aimed to explore the impact of the heave plate's diameter on the amplitude of the transitional motions of a 3-straked MCC with a low aspect ratio under the marine current and regular waves. Different heave plate configurations were simulated, with varying diameters while keeping other factors constant. The results showed that increasing the heave plate's diameter reduced the amplitude of the transitional motions. The use of a strake plate had an effect on reducing the amplitude of surge, sway, and heave motions, and the effect of using the heave plate was not specific to heave motion. Hence, with an optimal diameter of the heave plate at the keel of the 3-straked MCC, it is possible to reduce the amplitude of the surge and sway motions. According to Table 10, 3-straked MCC+ heave plates with diameters of $1.2D_{MCC}$-$1.4D_{MCC}$ had an acceptable performance in reducing the amplitude of the transitional

motions of the 3-straked MCC under both marine currents and regular waves. Hence, this numerical study showed that the effect of the strake plate is not only in reducing the amplitude of surge and sway motions but also the strake plate reduces the amplitude of heave motion. Also, the heave plate does not only have an effect on decreasing the amplitude of the heave motion but using an optimal diameter of the heave plate causes a noticeable reduction in the amplitude of the surge and sway motions. Nevertheless, the strake plates play a crucial role in mitigating the vortex shedding phenomenon by substantially altering the flow separation angle in the wake layer. This alteration effectively prevents the interaction of the shear layers on both sides of the MCC in the downstream.

Declaration of competing interest

The authors declare that they have no known competing financial interests or personal relationships that could have appeared to influence the work reported in this paper.

Funding

There are no financial support and funding for this research.

Data availability

Data will be made available on request.

Authors' contributions

Mahdi Bandizadeh Sharif: Conceptualization, Methodology, Software, Formal analysis, Validation, Writing original draft.
Hassan Ghassemi: Advisor, Scientific discussion, Analysis and assessment, Review & editing.
Guanghua He: Scientific discussion, Analysis and assessment, Review & editing.
Pengfei Liu: Scientific discussion, Analysis and assessment, Review & editing.

https://orcid.org/0000-0002-6201-346X (Hassan Ghassemi)
https://orcid.org/0009-0009-2897-9074 (Mahdi Bandizadeh Sharif)
https://orcid.org/0000-0001-9494-4712 (Guanghua He)

References

Agarwal, A. and A. Jain, "Dynamic behavior of offshore spar platforms under regular sea waves," Ocean Engineering 30 (4), 487-516 (2003). https://doi.org/10.1016/S0029-8018(02)00034-3

Ali, B., F. Ardhianutama, E. Djatmiko, N. Syahroni, Y. Mulyadi, R. Riyanto, R. Prastianto, and I. Rochani, "Experimental study on heave damping due to the heave plate addition on the SPAR keel," IOP Conference Series: Earth and Environmental Science 649 (1), 012052 (2021). https://doi.org/10.1088/1755-1315/649/1/012052

Atluri, S., J. Halkyard, and S. Sirnivas, "CFD simulation of truss spar vortex-induced motion," International Conference on Offshore Mechanics and Arctic Engineering 47497, 787-793 (2006). https://doi.org/10.1115/OMAE2006-92400

Bandizadeh Sharif, M., H. Ghassemi, G. He, and M. Karimirad, "A review of the flow-induced vibrations (FIV) in marine circular cylinder (MCC) fitted with various suppression devices," Ocean Engineering (2023). https://doi.org/10.1016/j.oceaneng.2023.116261

Banerjee, A., P. S. Gurugubelli, N. Kumar, and R. K. Jaiman, "Influence of flexible fins on vortex-induced load over a circular cylinder at low Reynolds number," Physics of Fluids 33 (11) (2021). https://doi.org/10.1063/5.0065562

Carlson, D. W. and Y. Modarres-Sadeghi, "Vortex-induced vibration of spar platforms for floating offshore wind turbines," Wind Energy 21 (11), 1169-1176 (2018). https://doi.org/10.1002/we.2221

CD-adapco., "User Guide - Star-CCM+ Version 8.02," (2013).

Ciba, E. and P. Dymarski, "Modelling of the viscosity effect of heave plates for floating wind turbines by hydrodynamic coefficients," acta mechanica et automatica 17 (3) (2023). https://doi.org/10.2478/ama-2023-0054

Ciba, E., "Heave motion of a vertical cylinder with heave plates," Polish Maritime Research (1), 42-47 (2021). https://doi.org/10.2478/pomr-2021-0004

Ciba, E., P. Dymarski, and M. Grygorowicz, "Heave Plates with Holes for Floating Offshore Wind Turbines," Polish Maritime Research (2022). https://doi.org/10.2478/pomr-2022-0003

DeMerchant, T., A. Magee, J. Penn, Z. Li, A. Loken, and S. Perryman, "Holstein spar hard tank strake structural design," Offshore Technology Conference (2005). https://doi.org/10.4043/17300-MS

Ding, Q., and C. Li, "Research on the influence of helical strakes on dynamic response of floating wind turbine platform," China Ocean Engineering 31, 131-140 (2017). https://doi.org/10.1007/s13344-017-0016-3

Ding, Q., C. Li, B. Li, W. Hao, and Z. Ye, "Research on the influence of helical strakes and its parameters on dynamic response of platform of floating wind turbine based on optimization method of orthogonal design," Journal of Solar Energy Engineering 139 (5), 051002 (2017). https://doi.org/10.1115/1.4037091

Fernandes, M. C., M. Saadat, P. Cauchy-Dubois, C. Inamura, T. Sirota, G. Milliron, H. Haj-Hariri, K. Bertoldi, and J. C. Weaver, "Mechanical and hydrodynamic analyses of helical strake-like ridges in a glass sponge," Journal of the Royal Society Interface 18 (182), 20210559 (2021). https://doi.org/10.1098/rsif.2021.0559

Finn, L., J. Maher, and H. Gupta, "The cell spar and vortex induced vibrations," Offshore Technology Conference, OTC-15244-MS (2003). https://doi.org/10.4043/15244-MS

Finnigan, T. and D. Roddier, "Spar VIM model tests at supercritical Reynolds numbers," International Conference on Offshore Mechanics and Arctic Engineering 4269, 731-740 (2007). https://doi.org/10.1115/OMAE2007-29160

Gonçalves, R. T., E. B. Malta, A. N. Simos, S. Hirabayashi, and H. Suzuki, "Experimental study of the effect of heave plate dimensions on the flow-induced motions (FIM) of a multi-column floating offshore wind turbine (FOWT)," International Conference on Offshore Mechanics and Arctic Engineering 85932, V008T009A050 (2022). https://doi.org/10.1115/OMAE2022-80344

Gonçalves, R. T., E. B. Malta, A. N. Simos, S. Hirabayashi, and H. Suzuki, "Influence of Heave Plate on the Flow-Induced Motions of a Floating Offshore Wind Turbine," Journal of Offshore Mechanics and Arctic Engineering 145 (3), 032001 (2023). https://doi.org/10.1115/1.4056345

Gonçalves, R. T., R. O. P. da Silva, M. A. Marques, S. Hirabayashi, G. R. da Silva Assi, A. N. Simos, and H. Suzuki, "Experimental study on vortex-induced motions of floating circular single cylinders with low aspect ratio and different heave plate geometries," ISOPE International Ocean and Polar Engineering Conference, ISOPE-I-20-3257 (2020).

Halkyard, J., J. Chao, P. Abbott, J. Dagleish, H. Banon, and K. Thiagarajan, "A deep draft semisubmersible with a retractable heave plate," Offshore technology conference, OTC-14304-MS (2002). https://doi.org/10.4043/14304-MS

Halkyard, J., S. Atluri, and S. Sirnivas, "Truss spar vortex induced motions: benchmarking of CFD and model tests," International Conference on Offshore Mechanics and Arctic Engineering 47497, 883-892 (2006). https://doi.org/10.1115/OMAE2006-92673

Halkyard, J., S. Sirnivas, S. Holmes, Y. Constantinides, O. H. Oakley Jr, and K. Thiagarajan, "Benchmarking of truss spar vortex induced motions derived from CFD with experiments," International Conference on

Offshore Mechanics and Arctic Engineering 41979, 895-902 (2005). https://doi.org/10.1115/OMAE2005-67252

Hegde, P. and S. Nallayarasu, "Hydrodynamic response of buoy form spar with heave plate near the free surface validated with experiments," Ocean Engineering 269, 113580 (2023). https://doi.org/10.1016/j.oceaneng.2022.113580

Hegde, P. and S. Nallayarasu, "Investigation of heave damping characteristics of buoy form spar with heave plate near the free surface using CFD validated by experiments," Ships and Offshore Structures, 1-18 (2022).

Holland, V., T. Tezdogan, and E. Oguz, "Full-scale CFD investigations of helical strakes as a means of reducing the vortex induced forces on a semi-submersible," Ocean Engineering 137, 338-351 (2017). https://doi.org/10.1016/j.oceaneng.2017.04.014

Hwang, J.-Y., K.-S. Yang, and S.-H. Sun, Reduction of flow-induced forces on a circular cylinder using a detached splitter plate, Physics of Fluids 15 (8), 2433-2436 (2003). https://doi.org/10.1063/1.1583733

Irani, M. and L. Finn, "Improved strake design for vortex induced motions of spar platforms," International Conference on Offshore Mechanics and Arctic Engineering 41952, 767-773 (2005). https://doi.org/10.1115/OMAE2005-67384

Irani, M. and L. Finn, "Model testing for vortex induced motions of spar platforms," International Conference on Offshore Mechanics and Arctic Engineering 37432, 605-610 (2004). https://doi.org/10.1115/OMAE2004-51315

Irani, M., S. Perryman, J. Brewer, and S. McNeill, "Vortex induced motions of the horn mountain truss spar," International Conference on Offshore Mechanics and Arctic Engineering 48210, 967-973 (2008). https://doi.org/10.1115/OMAE2008-57992

Ishihara, T., M. B. Waris, and H. Sukegawa, "A study on influence of heave plate on dynamic response of floating offshore wind turbine system," Proc. of European Offshore Wind Conference & Exhibition (2009).

Jang, H.-K., S. Park, M.-H. Kim, K.-H. Kim, and K. Hong, "Effects of heave plates on the global performance of a multi-unit floating offshore wind turbine," Renewable energy 134, 526-537 (2019). https://doi.org/10.1016/j.renene.2018.11.033

Kharazmi, R. and M. J. Ketabdari, "Numerical modeling to develop strake design of Spar platform for Vortex-Induced motions suppression," Ocean Engineering 250, 111060 (2022). https://doi.org/10.1016/j.oceaneng.2022.111060

Lake, M., H. He, A. W. Troesch, M. Perlin, and K. P. Thiagarajan, "Hydrodynamic coefficient estimation for TLP and Spar structures, "J. Offshore Mech. Arct. Eng. 122 (2), 118-124 (2000). https://doi.org/10.1115/1.533733

Lam, K. M., J. Hu, and P. Liu, "Vortex formation processes from an oscillating circular cylinder at high Keulegan–Carpenter numbers," Physics of fluids 22 (1) (2010). https://doi.org/10.1063/1.3291069

Lefevre, C., Y. Constantinides, J. W. Kim, M. Henneke, R. Gordon, H. Jang, and G. Wu, "Guidelines for CFD simulations of spar VIM," International Conference on Offshore Mechanics and Arctic Engineering 55416, V007T008A019 (2013). https://doi.org/10.1115/OMAE2013-10333

Li, B., Z. Huang, Y. M. Low, and J. Ou, "Experimental and numerical study of the effects of heave plate on the motion of a new deep draft multi-spar platform," Journal of marine science and technology 18, 229-246 (2013). https://doi.org/10.1007/s00773-012-0203-0

Li, J., S. Liu, M. Zhao, and B. Teng, "Experimental investigation of the hydrodynamic characteristics of heave plates using forced oscillation," Ocean Engineering 66, 82-91 (2013). https://doi.org/10.1016/j.oceaneng.2013.04.012

Li, X., Q. Xiao, E. Wang, C. Peyrard, and R. T. Gonçalves, "The dynamic response of floating offshore wind turbine platform in wave–current condition," Physics of Fluids 35 (8) (2023). https://doi.org/10.1063/5.0158917

Liang, H.-z., K. Liu, L.-y. Li, and J.-p. Ou, "Dynamic performance analysis of the tuned heave plate system for semi-submersible platform," China Ocean Engineering 32, 422-430 (2018). https://doi.org/10.1007/s13344-018-0044-7

Liu, J., W. Ma, L. Jin, X. Liu, and T. Li, "Experimental and numerical investigation on the wake flow and vortex shedding of a rotating circular cylinder," Physics of Fluids 35 (7) (2023). https://doi.org/10.1063/5.0157682

Lopez-Pavon, C. and A. Souto-Iglesias, "Hydrodynamic coefficients and pressure loads on heave plates for semi-submersible floating offshore wind turbines: A comparative analysis using large scale models," Renewable Energy 81, 864-881 (2015). https://doi.org/10.1016/j.renene.2015.04.003

Lopez-Pavon, C., C. A. Garrido-Mendoza, and A. Souto-Iglesias, "Hydrodynamic forces and pressure loads on heave plates for semi-submersible floating offshore wind turbines: A case study," International Conference on Offshore Mechanics and Arctic Engineering 45547, V09BT09A024 (2014). https://doi.org/10.1115/OMAE2014-24163

Mello PC, Malta EB, da Silva RO, et al. Influence of heave plates on the dynamics of a floating offshore wind turbine in waves. Journal of Marine Science and Technology 2021; 26: 190-200. https://doi.org/10.1007/s00773-020-00728-3

Mello, PC., E. B. Malta, R. O. da Silva, M. H. Candido, L. H. S. do Carmo, I. F. Alberto, G. R. Franzini, A. N. Simos, R. T. Gonçalves, and H. Suzuki, "2019A-IS2-3 Influence of Heave Plates on the Dynamics of a Floating Offshore Wind Turbine in Waves," Conference Proceedings The Japan Society of Naval Architects and Ocean Engineers 29, 69-77 (2019).

Moreno, J., K. P. Thiagarajan, and M. Cameron, "Hydrodynamic Coefficients of Hexagonal Heave Plates for Floating Offshore Wind Turbine Platforms," International Conference on Offshore Mechanics and Arctic Engineering 49972, V006T009A032 (2016). https://doi.org/10.1115/OMAE2016-54139

Murdjito, G. A. N., E. B. Djatmiko, and B. Ali, "Experimental Study of the Effect of Waves on SPAR Responses with and without Heave Plate in Intact and Damaged Mooring Systems," (2021). https://doi.org/10.5220/0010060101810190

Nallayarasu, S. and K. Bairathi, "Hydrodynamic response of spar hulls with heave damping plate using simplified approach," Ships and Offshore Structures 9 (4), 418-432 (2014). https://doi.org/10.1080/17445302.2013.841331

Nguyen, Q. D., W. Lu, L. Chan, A. Ooi, and C. Lei, "A state-of-the-art review of flows past confined circular cylinders," Physics of Fluids 35 (7) (2023). https://doi.org/10.1063/5.0157470

Oakley Jr, O. H. and Y. Constantinides, "CFD truss spar hull benchmarking study," International Conference on Offshore Mechanics and Arctic Engineering 4269, 703-713 (2007). https://doi.org/10.1115/OMAE2007-29150

Oakley Jr, O. H., Y. Constantinides, C. Navarro, and S. Holmes, "Modeling vortex induced motions of spars in uniform and stratified flows," International Conference on Offshore Mechanics and Arctic Engineering 41979, 885-894 (2005). https://doi.org/10.1115/OMAE2005-67238

Pang, D., L. Cheng, H. Jiang, F. Tong, and H. An, "Suppression of vortex shedding in the wake of a circular cylinder through high-frequency in-line oscillation," Physics of Fluids 35 (7) (2023). https://doi.org/10.1063/5.0155066

Rao, M. J., S. Nallayarasu, and S. Bhattacharyya, "CFD approach to heave damping of spar with heave plates with experimental validation," Applied Ocean Research 108, 102517 (2021). https://doi.org/10.1016/j.apor.2020.102517

Roddier, D., T. Finnigan, and S. Liapis, "Influence of the Reynolds number on spar vortex induced motions (VIM): multiple scale model test comparisons," International Conference on Offshore Mechanics and Arctic Engineering 43451, 797-806 (2009). https://doi.org/10.1115/OMAE2009-79991

Soeb, M. R., A. S. Islam, M. Z. Jumaat, N. Huda, and F. Arzu, "Response of nonlinear offshore spar platform under wave and current," Ocean Engineering 144, 296-304 (2017). https://doi.org/10.1016/j.oceaneng.2017.07.042

Subbulakshmi, A. and R. Sundaravadivelu, "Effects of damping plate position on heave and pitch responses of spar platform with single and double damping plates under regular waves," Ocean Engineering 224, 108719 (2021). https://doi.org/10.1016/j.oceaneng.2021.108719

Subbulakshmi, A. and R. Sundaravadivelu, "Heave damping of spar platform for offshore wind turbine with heave plate," Ocean Engineering 121, 24-36 (2016). https://doi.org/10.1016/j.oceaneng.2016.05.009

Subbulakshmi, A., J. Jose, R. Sundaravadivelu, and R. P. Selvam, "Effect of viscous damping on hydrodynamic response of spar with heave plate," Aquatic Procedia 4, 508-515 (2015). https://doi.org/10.1016/j.aqpro.2015.02.066

Sudhakar, S. and S. Nallayarasu, "Hydrodynamic response of spar with single and double heave plates in regular waves," International Journal of Ocean System Engineering 3 (4), 188-208 (2013). http://dx.doi.org/10.5574/IJOSE.2012.3.4.188

Sudhakar, S. and S. Nallayarasu, "Hydrodynamic responses of spar hull with single and double heave plates in random waves," International Journal of Ocean System Engineering 4 (1), 1-18 (2014). http://dx.doi.org/10.5574/IJOSE.2014.4.1.001

Sudhakar, S. and S. Nallayarasu, "Influence of heave plate on hydrodynamic response of spar," International Conference on Offshore Mechanics and Arctic Engineering 44335, 437-447 (2011). https://doi.org/10.1115/OMAE2011-49565

Sun, X., C. S. Suh, Z.-H. Ye, and B. Yu, Dynamics of a circular cylinder with an attached splitter plate in laminar flow: A transition from vortex-induced vibration to galloping, Physics of Fluids 32 (2) (2020). https://doi.org/10.1063/1.5125588

Takata, T., M. Takaoka, H. Houtani, K. Hara, S. Oh, E. B. Malta, K. Iijima, H. Suzuki, and R. T. Gonçalves, "Effect of Heave Plates on the Wave Motion of a Flexible Multicolumn FOWT," Energies 15 (20), 7605 (2022). https://doi.org/10.3390/en15207605

Tallavajhula, S., J. Wang, and I. Solberg, "Strength and Fatigue Analysis of VIM Suppression Strakes for Large Diameter Spars," International Conference on Offshore Mechanics and Arctic Engineering 42673, 67-76 (2007). https://doi.org/10.1115/OMAE2007-29078

Tao, L. and S. Cai, "Heave motion suppression of a Spar with a heave plate," Ocean engineering 31 (5-6), 669-692 (2004). https://doi.org/10.1016/j.oceaneng.2003.05.005

Thiagarajan, K., I. Datta, A. Z. Ran, L. Tao, and J. E. Halkyard, "Influence of heave plate geometry on the heave response of classic spars," International Conference on Offshore Mechanics and Arctic Engineering 36118, 621-627 (2002). https://doi.org/10.1115/OMAE2002-28350

Thiagarajan, K., Y. Constantinides, and L. Finn, "CFD analysis of vortex-induced motions of bare and straked cylinders in currents," International Conference on Offshore Mechanics and Arctic Engineering 41979, 903-908 (2005). https://doi.org/10.1115/OMAE2005-67263

Tian, X., J. Yang, X. Li, and T. Peng, "Experimental investigations on the hydrodynamic characteristics of heave plate," International Conference on Offshore Mechanics and Arctic Engineering 55393, V005T006A032 (2013). https://doi.org/10.1115/OMAE2013-10437

Van Dijk, R., A. Magee, S. van Perryman, and J. van Gebara, "Model test experience on vortex induced vibrations of truss spars," Offshore Technology Conference, OTC-15242-MS (2003). https://doi.org/10.4043/15242-MS

Wang, Y., J. Yang, T. Peng, and H. Lu, "Strake design and VIM-suppression study of a cell-truss spar," International Conference on Offshore Mechanics and Arctic Engineering 49149, 507-513 (2010). https://doi.org/10.1115/OMAE2010-20225

Yawar, A., F. Salehi, and S. Manzoor, "Lock-on to quasi-periodic flow transformation for a rotationally oscillating cylinder due to gust impulse," Physics of Fluids 35 (7) (2023). https://doi.org/10.1063/5.0157464

Yuan, H., J. Kou, C. Gao, and W. Zhang, "Resolvent and dynamic mode analysis of flow past a square cylinder at subcritical Reynolds numbers," Physics of Fluids 35 (7) (2023). https://doi.org/10.1063/5.0160274

Yue, M., Q. Liu, C. Li, Q. Ding, S. Cheng, and H. Zhu, "Effects of heave plate on dynamic response of floating wind turbine Spar platform under the coupling effect of wind and wave," Ocean Engineering 201, 107103 (2020). https://doi.org/10.1016/j.oceaneng.2020.107103

Zhang, S. and T. Ishihara, "Numerical study of distributed hydrodynamic forces on a circular heave plate by large-eddy simulations with volume of fluid method," Ships and Offshore Structures 15 (6), 574-586 (2020). https://doi.org/10.1080/17445302.2019.1661630

Zhang, S. and T. Ishihara, "Numerical study of distributed hydrodynamic forces on circular heave plates by large eddy simulations," Grand Renewable Energy proceedings Japan council for Renewable Energy (2018), 176 (2018). https://doi.org/10.24752/gre.1.0_176

Zhu, L. and H.-C. Lim, "Hydrodynamic characteristics of a separated heave plate mounted at a vertical circular cylinder," Ocean Engineering 131, 213-223 (2017). https://doi.org/10.1016/j.oceaneng.2017.01.007

Nomenclatures:

The following symbols are used in this paper:

$\dot{A}_0$: Initial velocity at t=0
$\dot{u}$: Horizontal acceleration (m/s^2)
$\dot{w}$: Vertical acceleration (m/s^2)
$\ddot{X}$: Acceleration in the surge direction
$\dot{X}$: Velocity in the surge direction
$\ddot{Y}$: Acceleration in the sway direction
$\dot{Y}$: Velocity in the sway direction
$\ddot{Z}$: Acceleration in the heave direction
$\dot{Z}$: Velocity in the heave direction
ρ_w: Fluid density (kg/m^3)
ω_d: Damping angular frequency (rad/s)
ω_n: Natural angular frequency (rad/s)
A(t): Free decay response
A: The maximum amplitude of the sway motion
A_0: Initial displacement at t=0
C: Damping coefficient (N.s/m)
C_0: Critical damping coefficient (N.s/m)
C_x: The damping in the X direction (N.s/m),
C_y: The damping in the Y direction (N.s/m)
C_z: The damping in the Z direction (N.s/m)
d: Depth (m)
D_{HP}: Heave plate diameter (m)
d_{MCC}: Draft of the MCC (m)
D_{MCC}: MCC's diameter (m)
$F_x(t)$: The force in the X direction (N)
$F_y(t)$: The force in the Y direction (N)
$F_z(t)$: The force in the Z direction (N)
H: Wave height (m)
H_0: Ring draft (m)
H_1: Force gauge height (m)

H_S: Strake's height (m)
K: Stiffness of the structure (N/m)
K: Wave number
K_x: The stiffness of the structure in the X direction (N/m)
K_y: The stiffness of the structure in the Y direction (N/m)
K_z: The stiffness of the structure in the Z direction (N/m)
L: Wave length (m)
L_{Box}: Box length
L_{Spring}: Spring length (m)
M: Mass of the structure (kg)
M_a: Added mass (kg)
N: Number of the strake
S_R: Scale ratio
S_{WP}: Water plane area (m^2)
T_d: Damping period (s)
t_{HP}: Thickness of the heave plate (m)
T_n: Natural period (s)
u: Horizontal velocity (m/s)
U_C: Velocity inlet of the marine current (m/s)
V_R: Reduced velocity (-)
w: Vertical velocity (m/s)
X: Surge motion
Y: Sway motion
Z: Heave motion
γ: Strake's pitch
η : Damping ratio
θ: Strake angle (degree)
a : Amplitude (m)
μ: Dynamic viscosity (kg/m. s)
ν: Kinematic viscosity (m^2/s)

Abbreviations:

The following symbols are used in this paper:

CF direction: Cross-Flow direction
CFD: Computational Fluid Dynamics
DES: Detached Eddy Simulation
DTBM: David Taylor Basin Model
FDT: Free Decay Test
FIV: Flow-Induced Vibrations
FSI: Fluid-Structure Interaction
FT: Berkeley, Force Technology
GoM: Gulf of Mexico
HP: Heave Plate
IL direction: In-Line direction
KC number: Keulegan-Carpenter number

LES: Large Eddy Simulation
MCC: Marine Circular Cylinder
RANS: Reynolds Averaged Navier-Stoke
RAO: Response Amplitude Operation
Re number: Reynolds number
ST number: Strouhal number
UC: University of California
VIM: Vortex-Induced-Motion
VOF: Volume of Fluid